# Chapter 8

# Cryogenics Instrumentation and Slow Controls

## 8.1 Introduction

The cryogenic instrumentation and slow controls (CISC) consortium provides comprehensive monitoring for all detector components and for liquid argon (LAr) quality and behavior as well as a control system for many detector components. The single-phase (SP) and dual-phase (DP) modules both use the same control system and have nearly identical cryogenics instrumentation except for differences in location due to the different time projection chamber (TPC) geometries and the addition of dedicated instrumentation for monitoring temperature and pressure in the gas phase for the DP module. Volume V, The DUNE Far Detector Dual-Phase Technology, Chapter 6 of this technical design report (TDR) is virtually the same as this chapter apart from those few differences.

The consortium responsibilities are split into two main branches: cryogenics instrumentation and slow controls, as illustrated in Figure 8.1.

Each element of CISC contributes to the DUNE physics program primarily through the maintenance of high detector live time. As described in Volume II, DUNE Physics, of this TDR, neutrino charge-parity symmetry violation (CPV) and resolution of the neutrino mass hierarchy over the full range of possible neutrino oscillation parameters will require at least a decade of running the far detector (FD). Similar requirements apply to searches for nucleon decay and supernova neutrino burst (SNB) events from within our galaxy. Throughout this long run-time the interior of any DUNE cryostat remains completely inaccessible. No possibility exists for repairs to any components that could be damaged within the TPC structure; hence environmental conditions that present risks must be detected and reported quickly and reliably.

Detector damage risks peak during the initial fill of a module with LAr, as temperature gradients take on their highest values during this phase. Thermal contractions outside of the range of design

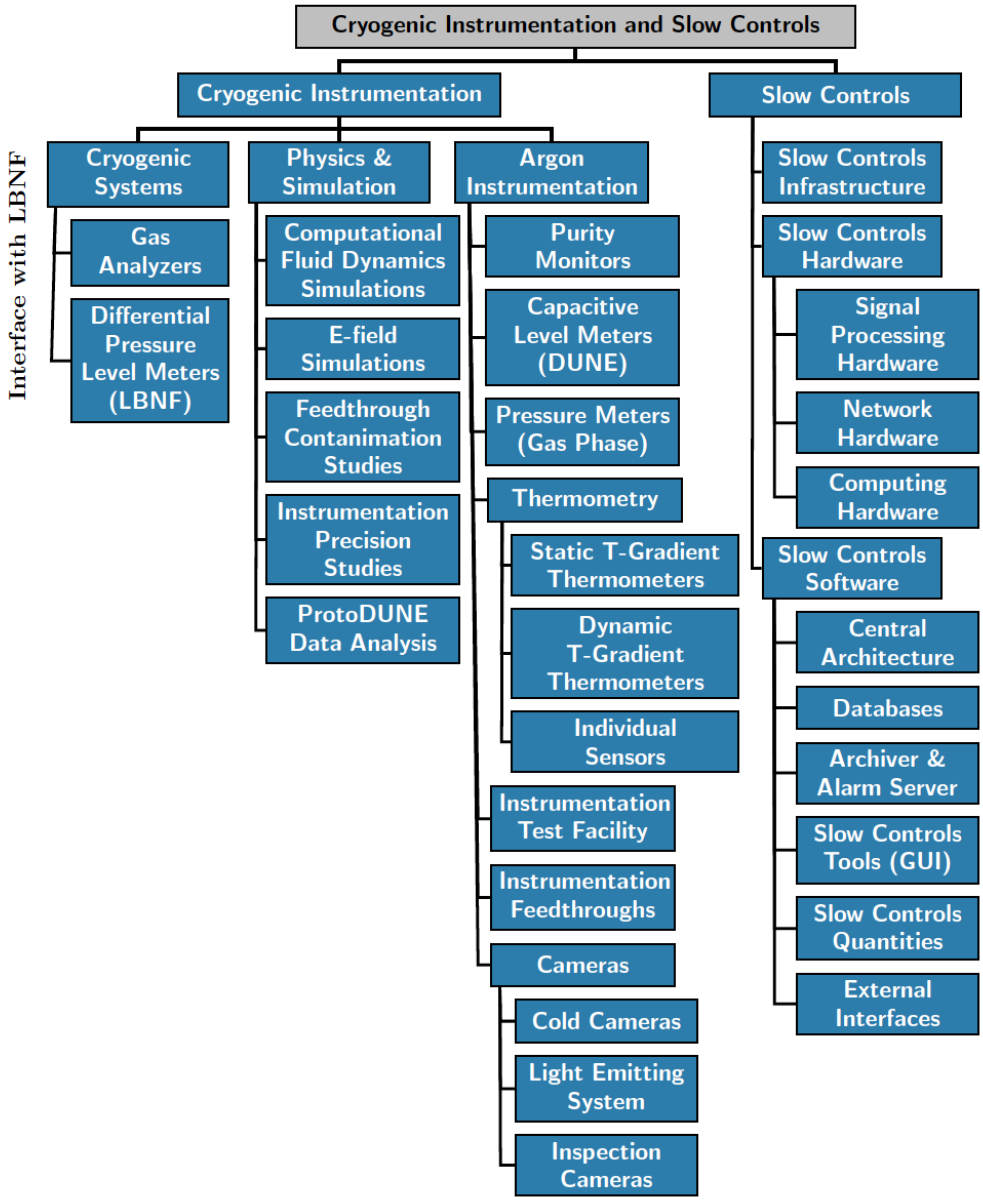


Figure 8.1: CISC subsystem chart

expectations could result in broken anode plane assembly (APA) wires, silicon photomultipliers (SiPMs) in photon detectors (PDs) that detach from the X-ARAPUCA light detectors, or poor connections at the cathode high voltage (HV) feedthrough point that could lead to unstable E fields. These considerations lead to the need for a robust temperature monitoring system for the detector, supplemented with liquid level monitors, and a high-performance camera system to enable visual inspection of the interior of the cryostat during the filling process. These systems are fully described in Section 8.2.1 of this chapter.

Argon purity must be established as early as possible in the filling process, a period in which gas analyzers are most useful, and must maintain an acceptable value, corresponding to a minimum electron drift lifetime of 3 ms, throughout the data-taking period. Dedicated purity monitors (Section 8.2.2) provide precise lifetime measurements up to values of 10 ms, the range over which electron attenuation most affects signal-to-noise (S/N) in the TPC. The purity monitors and gas analyzers remain important even after high lifetime has been achieved as periodic detector "top-off" fills occur; the new LAr must be of very high quality as it is introduced into the cryostat.

The CISC system must recognize and prevent fault conditions that could develop in the detector module over long periods of running. For example, the liquid level monitors must register any drop in liquid level; a drop in the level could place top sections of the field cage (FC) or bias HV points for the APAs close enough to the gas-liquid boundary to trigger sparking events. Very slow-developing outgassing phenomena could conceivably occur, with associated bubble generation creating another source of HV breakdown events. The cold camera system enables detection and identification of bubbling sites, and the development of mitigation strategies such as lower HV operation for some period of time. A more subtle possibility is the formation of quasi-stable eddies in argon fluid flow that could prevent positive argon ions from being cleared from the TPC volume, resulting in space charge build up that would not otherwise be expected at the depth of the FD. The space charge could in turn produce distortions in the TPC drift field that degrade tracking and calorimetry performance. The high-performance thermometry of the DUNE CISC system creates input for well developed complex fluid flow models described in Section 8.1.3 that should enable detection of conditions associated with these eddies.

Finally, a high detector live-time fraction over multi-year operation cannot be achieved without an extensive system to monitor all aspects of detector performance, report this information in an intelligent fashion to detector operators, and archive the data for deeper offline studies. Section 8.1.1.2 details the DUNE slow controls system designed for this task.

The baseline designs for all the CISC systems have been used in ProtoDUNE-SP, and most design parameters are extrapolated from these designs. The ProtoDUNE-SP data (and in some cases ProtoDUNE-DP data) will therefore be used to validate the instrumentation designs and to understand their performance.

### 8.1.1 Scope

#### 8.1.1.1 Cryogenics Instrumentation

Cryogenics instrumentation includes purity monitors, various types of temperature monitors, and cameras with their associated light emitting systems. Also included are gas analyzers and LAr level monitors that are directly related to the external cryogenics system, which have substantial interfaces with the Long-Baseline Neutrino Facility (LBNF). LBNF provides the needed expertise for these systems and is responsible for the design, installation, and commissioning, while the CISC consortium provides the resources and supplements labor as needed.

A cryogenic instrumentation test facility (CITF) for the instrumentation devices is also part of the cryogenics instrumentation. CISC is responsible for design through commissioning in the SP module of LAr instrumentation devices: purity monitors, thermometers, capacitive level meters, cameras, and light-emitting system, and their associated feedthroughs.

Cryogenics instrumentation requires significant engineering, physics, and simulation work, such as E field simulations and cryogenics modeling studies using computational fluid dynamics (CFD). E field simulations identify desirable locations for instrumentation devices in the cryostat, away from regions of high E field, so that their presence does not induce large field distortions. CFD simulations help identify expected temperature, impurity, and velocity flow distributions and guide the placement and distribution of instrumentation devices inside the cryostat.

#### 8.1.1.2 Slow Controls

The slow controls portion of CISC consists of three main components: hardware, infrastructure, and software. The slow controls hardware and infrastructure comprises networking hardware, signal processing hardware, computing hardware, and associated rack infrastructure. The slow controls software provides, for every slow control quantity, the central slow controls processing architecture, databases, alarms, archiving, and control room displays.

CISC provides software and infrastructure for controlling and monitoring all detector elements that provide data on the health of the detector module or conditions important to the experiment, as well as some related hardware.

Slow controls base software and databases are the central tools needed to develop control and monitoring for various detector systems and interfaces. These include:

- base input/output software;
- alarms, archiving, display panels, and similar operator interface tools; and
- slow controls system documentation and operations guidelines.

Slow controls for external systems collect data from systems external to the detector module

and provide status monitoring for operators and archiving. They collect data on beam status, cryogenics status, data acquisition (DAQ) status, facilities systems status, interlock status bit monitoring (but not the actual interlock mechanism), ground impedance monitoring, and possibly building and detector hall monitoring, as needed.

The DUNE detector safety system (DDSS) can provide inputs to CISC on safety interlock status, and CISC will monitor and make that information available to the experiment operators and experts as needed. However, DDSS and CISC are separate monitors, and the slow controls portion of CISC does not provide any inputs to DDSS. A related question is whether CISC can provide software intervention before a hardware safety interlock. In principle such intervention can be implemented in CISC, presumably by (or as specified by) the hardware experts. For example, at ProtoDUNE-SP, the automatic lowering of HV to clear streamers was implemented in the software for the HV control using CISC-level software.

Slow controls covers software interfaces for detector hardware devices, including:

- monitoring and control of all power supplies,
- full rack monitoring (rack fans, thermometers and rack protection system),
- instrumentation and calibration device monitoring (and control to the extent needed),
- power distribution unit and computer hardware monitoring,
- HV system monitoring through cold cameras, and
- detector components inspection using warm cameras.

CISC will develop, install, and commission any hardware related to rack monitoring and control. Most power supplies may only need a cable from the device to an Ethernet switch, but some power supplies might need special cables (e.g., GPIB or RS232) for communication. The CISC consortium is responsible for providing these control cables.

CISC has additional activities outside the scope of the consortium that require coordination with other groups. This is discussed in Section 8.4.4.

### 8.1.2 Design Considerations

Important design considerations for instrumentation devices include stability, reliability, and longevity, so that devices can survive for at least 20 years. Such longevity is uncommon for any device, so the overall design allows replacement of devices where possible. Some devices are critical for filling and commissioning but less critical for later operations; for these devices we specify a minimum lifetime of 18 months and 20 years as a desirable goal. DUNE requires the E field on any instrumentation devices inside the cryostat to be less than 30 kV/cm to minimize the risk of dielectric breakdown in LAr.

A consideration important for event reconstruction is the maximum noise level induced by instrumentation devices that the readout electronics can tolerate. ProtoDUNE-SP is evaluating this.

Table 8.1 shows the top-level specifications that determine the requirements for CISC together with selected high-level specifications for CISC subsystems. The physics-driven rationale for each requirement and the proposed validation are also included in the table. Tables 8.2 and 8.3 show the full set of specifications for the CISC subsystems. In all these tables two values are quoted for most of the design parameters: (1) specification, which is the intended value or limits for the parameter set by physics and engineering needs, and (2) goal, an improved value offering a benefit which the collaboration aims to achieve where it is cost-effective to do so.

Data from purity monitors and different types of thermometers will be used to validate the LAr fluid flow model. A number of requirements drive the design parameters for the precision and granularity of monitor distribution across the cryostat. For example, the electron lifetime measurement precision must be 1.4 % to keep the bias on the charge readout in the TPC below 0.5 % at 3 ms lifetime. For thermometers, the parameters are driven by the CFD simulations based on ProtoDUNE-SP design. The temperature measurement resolution must be less than 2 mK, and the relative precision of those measurements must be less than 5 mK. The resolution is defined as the temperature root mean square (RMS) for individual measurements and is driven by the electronics. The relative precision also includes the effect of reproducibility for successive immersions in LAr. The relative precision is particularly important in order to characterize gradients below 20 mK. As will be described below, the laboratory calibration data and the recent analysis of thermometer instrumentation data from ProtoDUNE-SP shows that a 2.5 mK relative precision is achievable.

The level meters must have a precision of 0.1% over 14 m (i.e., 14 mm) for measurement accuracy during filling. This precision is also sufficient to ensure that the LAr level stays above the ground planes (GPs) of a single-phase (SP) module. As shown in Table 8.3, several requirements drive the design of cold and warm cameras and the associated light emitting system. The components of the camera systems must not contaminate the LAr or produce bubbles so as to avoid increasing the risk of HV discharge. Both cold and warm cameras must provide coverage of at least 80 % of the TPC volume with a resolution of 1 cm for cold cameras and 2 mm for warm cameras on the TPC.

For the CITF, a cryostat with a capacity of only 0.5 to approximately 3 $m^3$ will suffice and will keep turn-around times and filling costs lower. For gas analyzers, the operating range must allow establishment of useful electron lifetimes; details are in Table 8.2.

For slow controls, the system must be sufficiently robust to monitor a minimum of 150,000 variables per detector module, and support a broad range of monitoring and archiving rates; the estimated variable count, data rate, and archive storage needs are discussed in Section 8.3.4. The system must also interface with a large number of detector subsystems and establish two-way communication with them for control and monitoring. For the alarm rate, 150 alarms/day is used as the specification as it is the maximum to which humans can be expected to respond. The goal for the alarm rate is less than 50 alarms/day. The alarm logic system will need to include features for managing “alarm storms” using alarm group acknowledgment, summaries, delays, and other aids.

Table 8.1: CISC specifications

| Label | Description | Specification (Goal) | Rationale | Validation |
|---|---|---|---|---|

| | | | | |
|---|---|---|---|---|
| SP-FD-5 | Liquid argon purity | $<100$ ppt ($<30$ ppt) | Provides >5:1 S/N on induction planes for pattern recognition and two-track separation. | Purity monitors and cosmic ray tracks |
| SP-FD-15 | LAr nitrogen contamination | $<25$ ppm | Maintain 0.5 PE/MeV PDS sensitivity required for triggering proton decay near cathode. | In situ measurement |
| SP-FD-18 | Cryogenic monitoring devices | | Constrain uncertainties on detection efficiency, fiducial volume. | ProtoDUNE |
| SP-FD-25 | Non-FE noise contributions | $<<1000\ e^-$ | High S/N for high reconstruction efficiency. | Engineering calculation and ProtoDUNE |
| SP-FD-29 | Detector uptime | $>98\%$ ($>99\%$) | Meet physics goals in timely fashion. | ProtoDUNE |
| SP-FD-30 | Individual detector module uptime | $>90\%$ ($>95\%$) | Meet physics goals in timely fashion. | ProtoDUNE |
| SP-CISC-1 | Noise from Instrumentation devices | $<<1000\ e^-$ | Max noise for 5:1 S/N for a MIP passing near cathode; per SBND and DUNE CE | ProtoDUNE |
| SP-CISC-2 | Max. E field near instrumentation devices | $<30$ kV/cm ($<15$ kV/cm) | Significantly lower than max field of 30 kV/cm per DUNE HV | 3D electrostatic simulation |
| SP-CISC-3 | Precision in electron lifetime | $<1.4\%$ ($<1\%$) | Required for accurate charge reconstruction per DUNE-FD Task Force report. | ProtoDUNE-SP and CITF |
| SP-CISC-4 | Range in electron lifetime | 0.04 ms to 10 ms in cryostat, 0.04 ms to 30 ms inline | Slightly beyond best values observed so far in other detectors. | ProtoDUNE-SP and CITF |
| SP-CISC-11 | Precision: temperature reproducibility | $<5$ mK (2 mK) | Enables validation of CFD models, which predicts gradients below 15 mK | ProtoDUNE-SP and CITF |
| SP-CISC-14 | Temperature stability | $<2$ mK at all places and times (Match precision requirement at all places, at all times) | Measure the temp map with sufficient precision during the entire duration | ProtoDUNE-SP |
| SP-CISC-27 | Cold camera coverage | $>80\%$ of HV surfaces (100%) | Enable detailed inspection of issues near HV surfaces. | Calculated from location, validated in prototypes. |
| SP-CISC-51 | Slow control alarm rate | $<150$/day ($<50$/day) | Alarm rate low enough to allow response to every alarm. | Detector module; depends on experimental conditions |
| SP-CISC-52 | Total No. of variables | $>150{,}000$ (150,000 to 200,000) | Scaled from ProtoDUNE-SP | ProtoDUNE-SP and CITF |
| SP-CISC-54 | Archiving rate | 0.02 Hz (Broad range 1 Hz to 1 per few min.) | Archiving rate different for each variable, optimized to store important information | ProtoDUNE-SP |

Table 8.2: List of specifications for the different CISC subsystems (1).

| **Quantity/Parameter** | Specification | Goal |
|---|---|---|
| Noise from Instrumentation devices | $\ll$ 1000 $e^-$ | |
| Max. E field near instrumentation devices | <30 kV/cm | <15 kV/cm |
| **Purity Monitors** | | |
| Precision in electron lifetime | <1.4% at 3 ms, <4% at 9 ms, relative differences <2.5% | < 1% |
| Range in electron lifetime | 0.04 - 10 ms | (0.04 - 30 ms inline) |
| Longevity | 20 years | > 20 years |
| Stability | Match precision requirement at all places/times | |
| Reliability | Daily Measurements | Measurements as needed |
| **Thermometers** | | |
| Vertical density of sensors for T-gradient monitors | > 2 sensor/m | > 4 sensors/m |
| 2D horizontal density for top/bottom individual sensors | 1 sensor/5(10) m | 1 sensor/3(5) m |
| Swinging/deflection of T-Gradient monitors | < 5 cm | < 2 cm |
| Resolution of temperature measurements | < 2 mK | <0.5 mK |
| Precision: temperature reproducibility | < 5 mK | 2 mK |
| Reliability | 80% (in 18 months) | 50% (during 20 years) |
| Longevity | > 18 months | > 20 years |
| Stability | < 2 mK at all places and times | Match precision requirement at all places/times |
| Discrepancy between lab and in situ calibrations for temperature sensors | < 5 mK | < 3 mK |
| Discrepancy between measured temperature map and CFD simulations in ProtoDUNE-SP | < 5 mK | |
| **Gas Analyzers** | | |
| Operating Range O2 | 0.2 (air) to 0.1 ppt | |
| Operating Range H2O | Nom. air to sub-ppb; contaminant-dependent | |
| Operating Range N2 | Nominally Air Nom. air to sub-ppb; contaminant-dependent | |
| Precision: 1 sigma at zero | per gas analyzer range | |
| Detection limit: 3 sigma | Different analyzer modules needed to cover entire range | |
| Stability | <% of full scale range. | |
| Longevity | >10 years | |
| **Pressure Meters (GAr)** | | |
| Relative precision (DUNE side) | 0.1 mbar | |

Table 8.3: List of specifications for the different CISC subsystems (2)

| **Quantity/Parameter** | Specification | Goal |
|---|---|---|
| **Level Meters** | | |
| Precision (LBNF scope) | 0.1% over 14 m (14 mm) | |
| Precision (capacitive level meters, Deep Underground Neutrino Experiment (DUNE) scope) | 1 cm | <5 mm |
| Longevity (all) | 20 years | > 20 years |
| **Cold cameras** | | |
| Coverage | 80% of the exterior of HV surfaces | 100% |
| Frames per second | yet to be defined | |
| Resolution | 1 cm on the TPC | yet to be defined |
| Duty cycle | yet to be defined | |
| longevity | > 18 months | > 20 years |
| **Inspection cameras** | | |
| Coverage | 80% of the TPC | yet to be defined |
| Frames per second | yet to be defined | |
| Resolution | 2 mm on the TPC | yet to be defined |
| heat transfer | no generation of bubbles | |
| longevity | > 18 months | > 20 years |
| **Light emitting system** | | |
| radiant flux | > 10 mW/sr | 100 mW/sr |
| power | < 125 mW/LED | |
| wavelength | red/green | IR/white |
| longevity | > 18 months (for cold cameras) | > 20 years |
| **cryogenic instrumentation test facility (CITF)** | | |
| Dimensions | 0.5 to 3 cubic meters | |
| Temperature stability | $\pm$1K | |
| Turn-Around time | $\sim$9 days | 9 days |
| LAr purity | O2, H2O: low enough to measure drifting electrons of devices under test, $\sim$ 0.5 ms. N2: ppm for scintillation light tests. | >1.0 ms |
| **Slow Controls** | | |
| Alarm rate | <150/day | < 50/day |
| Total No. of variables per detector module | 150,000 | 150,000 - 200,000 |
| Server rack space | 2 racks | 3 racks |
| Archiving rate | 0.02 Hz | Broad range 1 Hz to 1 per few min. |
| Near Detector Status | Beam conditions and detector status | Full beam and detector status |

### 8.1.3 Fluid Dynamics Simulation

Proper placement of purity monitors, thermometers, and liquid level monitors within the detector module requires knowing how LAr flows within the cryostat, given its fluid dynamics, heat and mass transfer, and distribution of impurity concentrations. Fluid flow is also important in understanding how the positive and negative ion excess created by various sources (e.g., ionization from cosmic rays and $^{36}$Ar) is distributed across the detector as it affects E field uniformity. Finally, CFD simulations are crucial to predict the purity of the argon in regions where experimental data is unavailable. The overall goal of the CFD simulations is to better understand and predict the fluid (in either liquid or vapor state) motions and the implications for detector performance.

Fluid motion within the cryostat is driven primarily by small changes in density caused by thermal gradients within the fluid although pump flow rates and inlet and outlet locations also contribute. Heat sources include exterior heat from the surroundings, interior heat from electronics, and heat flow through the pump inlet. In principle, purity monitors can be placed throughout the cryostat to determine if the argon is pure enough for experimentation. However, some areas inside the cryostat are off limits for such monitors.

The fluid flow behavior can be determined by simulating LAr flow within a detector module using Siemens Star-CCM+[1], a commercially available CFD code. Such a model must properly define the fluid characteristics, solid bodies, and fluid-solid interfaces, as well as provide a way to measure contamination, while still maintaining reasonable computation times. In addition, these fluid dynamics simulations can be compared to available experimental data to assess simulation accuracy and credibility.

Although simulation of the detector module presents challenges, acceptable simplifications can accurately represent the fluid, the interfacing solid bodies, and variations of contaminant concentrations. Because of the magnitude of thermal variation within the cryostat, modeling of the LAr is simplified by using constant thermophysical properties, calculating buoyant force with the Boussinesq Model (using a constant density for the fluid with application of a temperature-dependent buoyant force), and a standard shear stress transport turbulence model. Solid bodies that touch the LAr include the cryostat wall, cathode planes, anode planes, GP, and FC. As in previous CFD models of the DUNE 35 ton prototype and ProtoDUNE-SP [159], the FC planes, anode planes, and GP can be represented by porous bodies. Because impurity concentration and electron lifetime do not affect fluid flow, these variables can be simulated as passive scalars, as is commonly done for smoke released [160] in air or dyes released in liquids.

Discrepancies between real data and simulations may affect detector performance. Simulation results contribute to decisions about where to place sensors and monitors, and to the definitions of various calibration quantities. Methods of mitigating such risks include well established convergence criteria, sensitivity studies, and comparison to results of previous CFD simulation work. Moreover, the simulation will be improved with input from LAr temperature and purity measurements and validation tests from ProtoDUNE-SP[2].

[1] https://mdx.plm.automation.siemens.com/star-ccm-plus

[2] Because ProtoDUNE-DP was not instrumented with high-precision thermometers in the liquid phase and because the cryogenics design is the same for SP and DP modules of the DUNE FD, ProtoDUNE-SP data will be used to validate

Taking into account that the CFD model can predict both temperature and impurity levels, the procedure for validating and tuning the CFD model will be the following: (1) use temperature measurements in numerous locations in the cryostat to constrain temperature predictions and improve the CFD model, (2) use the improved model to predict the LAr impurity level at the purity monitor locations, and (3) compare the predictions to the actual purity monitor measurements to further constrain the CFD model.

Figure 8.2 shows an example of the temperature distribution on a plane intersecting a LAr inlet and at a plane halfway between an inlet and an outlet; the geometry used for this simulation is shown in Figure 8.3[3]. Note the plume of higher temperature LAr between the walls and the outer APA on the inlet plane. The current placement of instrumentation in the cryostat as shown in Figure 8.5 was determined using temperature and impurity distributions from previous simulations.

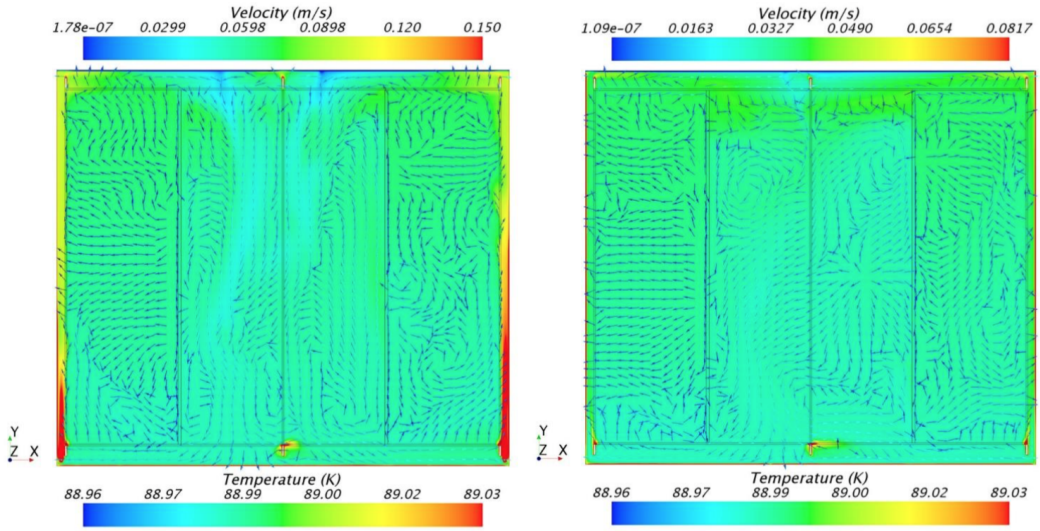


Figure 8.2: Distribution of temperature on a plane intersecting an inlet (left) and halfway between an inlet and an outlet (right), as predicted by previous CFD simulations (from [159]). (See Figure 8.3 for geometry.)

The strategy for future CFD simulations begins with understanding the performance of the ProtoDUNE-SP cryogenics system and modeling the detector modules to derive specifications for instrumentation. We are pursuing a prioritized set of studies to help determine the requirements for other systems. We plan to

- Review the DUNE FD cryogenics system design and verify the current implementation in simulation to ensure that the simulation represents the actual design.
- Model the ProtoDUNE-SP liquid and gas regions with the same precision as the FD. Presently, we have only the liquid model, which is needed to interpret the thermometer data. The gas model is needed to see how to place thermometers in the ullage and verify the design of the gaseous argon purge system.

the liquid CFD model.

[3]The inlet and outlet map has recently changed; it now consists of two rows of 64 inlets each at each longer side of the cryostat and four outlets along the shorter sides (drift direction) of the cryostat.

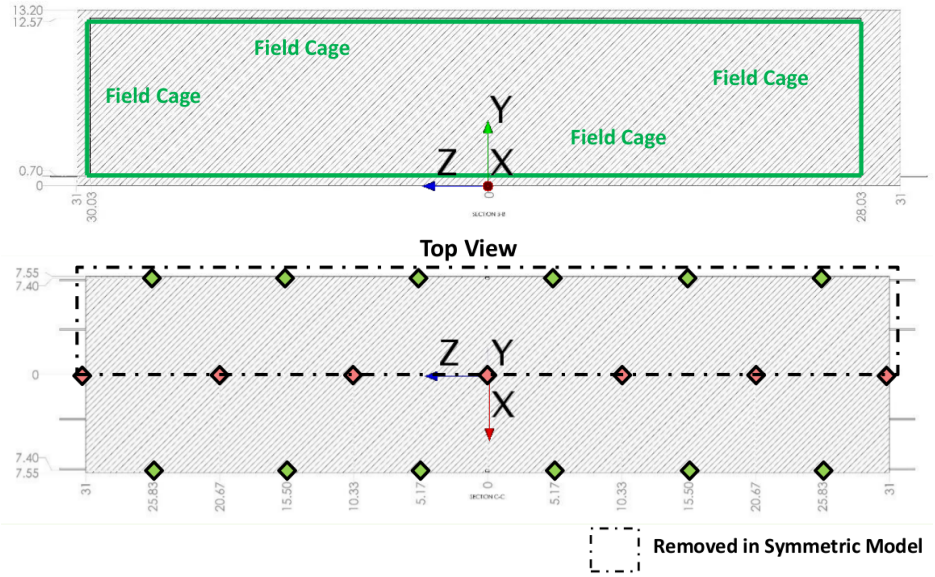


Figure 8.3: Layout of the SP module within the cryostat (top) and positions of LAr inlets and outlets (bottom) as modeled in the CFD simulations [159]. The $y$ axis is vertical and the $x$ axis is parallel to the TPC drift direction. Inlets are shown in green and outlets are shown in red.

- Verify the CFD model for the SP module in a simulation performed by LBNF; this defines the requirements for instrumentation devices (e.g., thermometry).

#### 8.1.3.1 Validation in ProtoDUNE

ProtoDUNE-SP has collected data to validate the CFD using:

- static and dynamic T-gradient thermometers,
- individual temperature sensors placed in the return LAr inlets,
- two 2D grids of individual temperature sensors installed below the bottom ground planes and above the top ground planes,
- a string of three purity monitors vertically spaced from near the bottom of the cryostat to just below the LAr surface,
- two pressure sensors (relative and absolute) in the argon gas,
- $H_2O$, $N_2$, and $O_2$ gas analyzers,
- LAr level monitors, and
- standard cryogenic sensors including pressure transducers, individual temperature sensors placed around the cryostat on the membrane walls, and recirculation flow rates transducers.

The data, which have been logged through the ProtoDUNE-SP slow control system [161], are available for offline analysis.

In parallel, CISC has produced a ProtoDUNE-SP CFD model with input from ProtoDUNE-SP

measurements (see Table 8.4). Streamlines[4] from the current simulation (Figure 8.4) show the flow paths from the four cryostat inlets to the outlet. The validation of this model consists of an iterative process in which several versions of the CFD simulation, using different input parameters, eventually converge to a reasonable agreement with data from instrumentation devices. Those comparisons will be shown in Section 8.2.1.4.

Table 8.4: CFD input parameters for ProtoDUNE-SP

| **Parameter** | Value | Comments |
|---|---|---|
| Cryostat height | 7.878 m | Measured with laser (1 cm error approx.) |
| LAr surface height | 7.406 m | Measured by capacitive level meter ($< 1$ cm error) |
| Ullage pressure | 1.045 bar | Measured by pressure gauges |
| LAr surface temperature | 87.596 K | Computed using ullage pressure and [162] |
| LAr inlet temperature | bulk LAr + 0.2 K | Estimated from pressure settings in cryo-system |
| LAr flow rate per pipe | 0.417 kg/s | Estimated from cryostat filling rate |

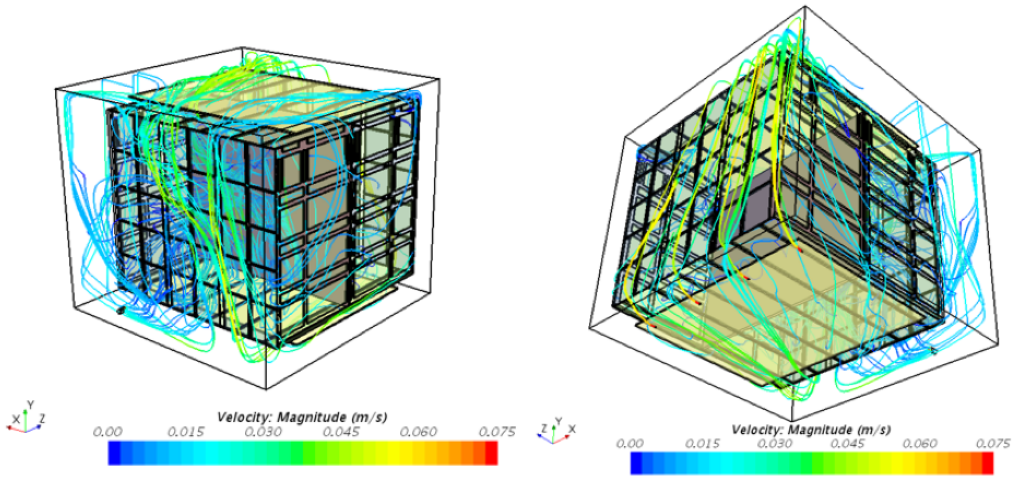


Figure 8.4: Streamlines for LAr flow inside ProtoDUNE-SP

Once the ProtoDUNE-SP CFD model predicts the fluid temperature in the entire cryostat to a reasonable level under different conditions, we will use it to produce maps of impurity levels in the detector module. These can be easily converted into electron lifetime maps, which we will compare to the ProtoDUNE-SP purity monitor data.

## 8.2 Cryogenics Instrumentation

Instrumentation inside the cryostat must accurately report the condition of the LAr so that we can ensure that it is adequate to operate the TPC. This instrumentation includes purity monitors

[4]In fluid mechanics, a streamline is a line that is everywhere tangent to the local velocity vector. For steady flows, a streamline also represents the path that a single particle of the fluid will take from inlet to exit.

to check the level of impurity in the argon and to provide high-precision electron lifetime measurements, as well as gas analyzers to verify that the levels of atmospheric contamination do not rise above certain limits during the cryostat purging, cooling, and filling. Temperature sensors deployed in vertical arrays and at the top and bottom of the detector module monitor the cryogenics system operation, providing a detailed 3D temperature map that helps predict the LAr purity across the entire cryostat. The cryogenics instrumentation also includes LAr level monitors and a system of internal cameras to help find sparks in the cryostat and to monitor the overall cryostat interior.

The proper placement of purity monitors, thermometers, and liquid-level monitors in the detector module requires understanding the LAr fluid dynamics, heat and mass transfer, and the distribution of impurity concentrations within the cryostat. Both this and coherent analysis of the instrumentation data require CFD simulation results.

ProtoDUNE-SP is testing the performance of purity monitors, thermometers, level monitors and cameras for the SP module, validating the baseline design.

### 8.2.1 Thermometers

As discussed in Section 8.1.3, a detailed 3D temperature map is important for monitoring the cryogenics system for correct functioning and the LAr for uniformity. Given the complexity and size of purity monitors, they can only be installed on the sides of the cryostat to provide a local measurement of LAr purity. A direct measurement of the LAr purity across the entire cryostat is not feasible, but a sufficiently detailed 3D temperature map based on CFD simulations can predict it. The vertical coordinate is especially important because it will relate closely to the LAr recirculation and uniformity.

The baseline sensor distribution and the cryostat ports used to extract cables (with indication of number of cables per port) are shown in Figure 8.5. The baseline distribution will evolve as more information becomes available (precise CFD simulations, better understanding of detector support system (DSS) ports, installation interfaces with other groups), but the baseline suffices to establish the overall strategy.

High-precision temperature sensors will be distributed near the TPC walls in two ways: (1) forming high density ($>$ 2 sensors/m) vertical arrays (called T-gradient monitors) and (2) in coarser ($\sim$ 1 sensor/5 m) 2D arrays (called individual sensors) at the top and bottom of the detector module, where it is most crucial to know the temperature.

Expected temperature variations inside the cryostat are very small (0.02 K; see Figure 8.2), so sensors must be cross-calibrated to better than 0.005 K. Most sensors will be calibrated in the laboratory before installation (installation is described in Section 8.4.5.2). Calibration before installation is the only option for sensors installed on the long sides of the detector and the top and bottom of the cryostat, where space is limited. Given the precision required and the unknown longevity of the sensors – possibly requiring another calibration after some time – an additional method will be used for T-gradient monitors installed on the short ends of the detector in the space

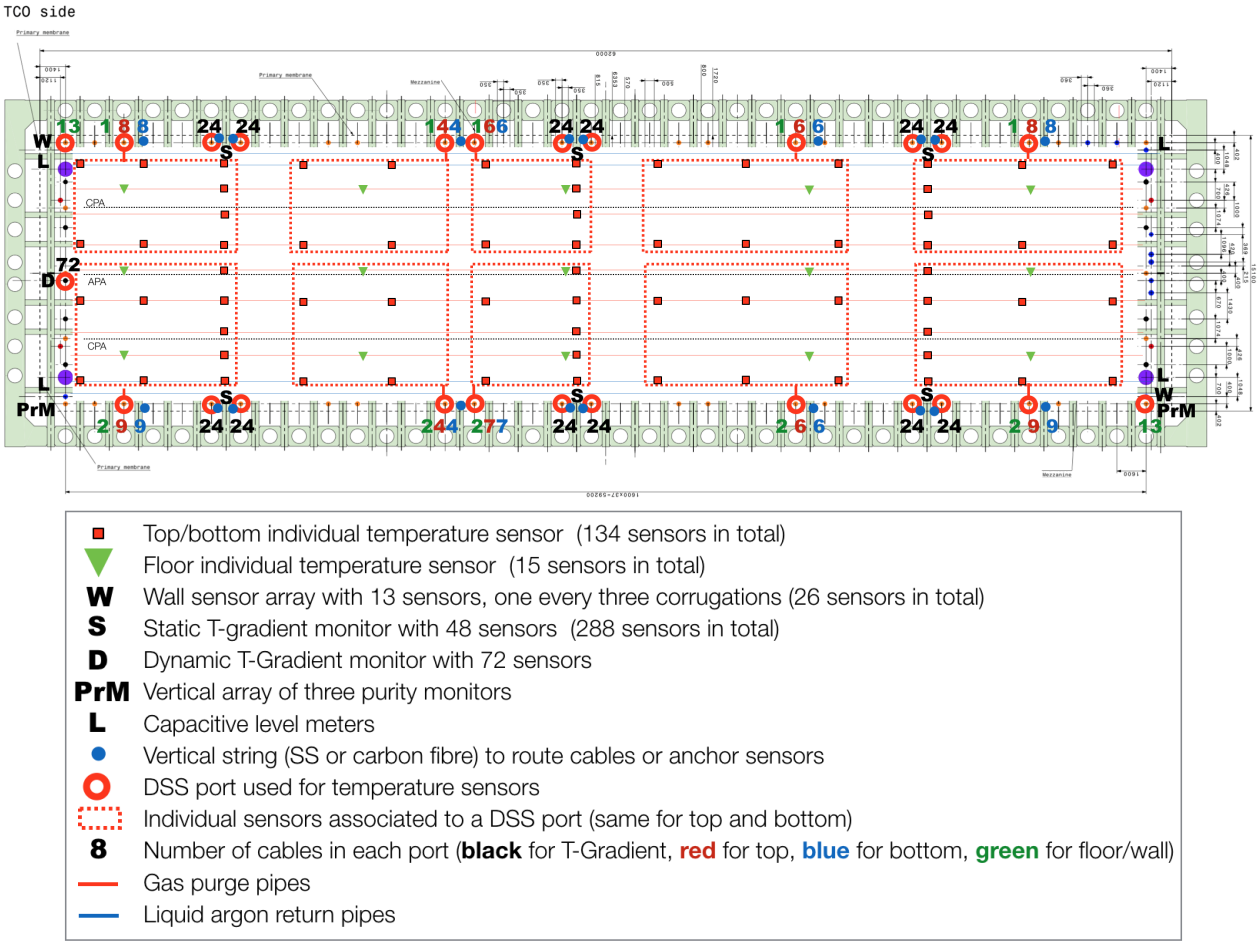


- Top/bottom individual temperature sensor (134 sensors in total)
- Floor individual temperature sensor (15 sensors in total)
- **W** Wall sensor array with 13 sensors, one every three corrugations (26 sensors in total)
- **S** Static T-gradient monitor with 48 sensors (288 sensors in total)
- **D** Dynamic T-Gradient monitor with 72 sensors
- **PrM** Vertical array of three purity monitors
- **L** Capacitive level meters
- Vertical string (SS or carbon fibre) to route cables or anchor sensors
- DSS port used for temperature sensors
- Individual sensors associated to a DSS port (same for top and bottom)
- **8** Number of cables in each port (**black** for T-Gradient, **red** for top, **blue** for bottom, **green** for floor/wall)
- Gas purge pipes
- Liquid argon return pipes

Figure 8.5: Distribution of temperature sensors inside the cryostat

between the field cage end walls and the cryostat walls. There is sufficient space in this area for a movable system, which can be used to cross calibrate the temperature sensors in situ, as described in 8.2.1.1.

The baseline design for all thermometer systems have three elements in common: sensors, cables, and readout system. We plan to use Lake Shore PT100-series[5] platinum sensors with 100 Ω resistance because in the temperature range 83 K to 92 K they show high reproducibility of ∼ 5 mK and absolute temperature accuracy of 100 mK. Using a four-wire readout greatly reduces issues related to lead resistance, any parasitic resistances, connections through the flange, and general electromagnetic noise pick-up. Lakeshore PT102 sensors (see Figure 8.13, right) were used in the 35 ton prototype and ProtoDUNE-SP, giving excellent results. For the inner readout cables, a custom cable made by Axon[6] is the baseline. It consists of four teflon-jacketed copper wires (American wire gauge (AWG) 28), forming two twisted pairs, with a metallic external shield and an outer teflon jacket. The readout system is described in Section 8.2.1.5.

Another set of lower-precision sensors epoxied into the bottom membrane of the cryostat will monitor the cryostat filling in the initial stage. Finally, the inner walls and roof of the cryostat will have the same types of sensors to monitor the temperature during cool-down and filling ("W" sensors in Figure 8.5).

#### 8.2.1.1 Dynamic T-gradient monitors

To address concerns about potential differences in sensor readings prior to and after installation in a detector module, and potential drifts over the lifetime of the module that may affect accuracy of the vertical temperature gradient measurement, a dynamic temperature monitor allows cross-calibration of sensor readings in situ. Namely, this T-gradient monitor is motorized, allowing vertical motion of the temperature sensor array in the detector module, enabling precise cross-calibration between the sensors, as illustrated in Figure 8.6.

The procedure for cross-calibrations is the following: in step 1, the temperature reading of all sensors is taken at the home (lowest) position of the carrier rod. In step 2, the stepper motor moves the carrier rod up 25 cm. Since the sensors along the entire carrier rod are positioned 25 cm apart, when the system is moved up 25 cm, each sensor is positioned at the height that was occupied by another sensor in step 1. Then a second temperature reading is taken. In this manner, except for the lowest position, two temperature measurements are taken at each location with different sensors. Assuming that the temperature at each location is stable over the few minutes required to make the measurements, any difference in the temperature readings between the two different sensors is due to their relative measurement offset. This difference is then calculated for all locations. In step 3, readout differences between pairs of sensors at each location are linked to one another, expressing temperature measurements at all heights with respect to a single sensor. In this way, temperature readings from all sensors are cross-calibrated in situ, canceling all possible offsets due to electromagnetic noise or any parasitic resistances that may have prevailed despite the four-point connection to the sensors that should cancel most of

[5] Lake Shore Cryotronics™ platinum RTD series, `https://www.lakeshore.com/`.

[6] Axon™ Cable, `http://www.axon-cable.com`.

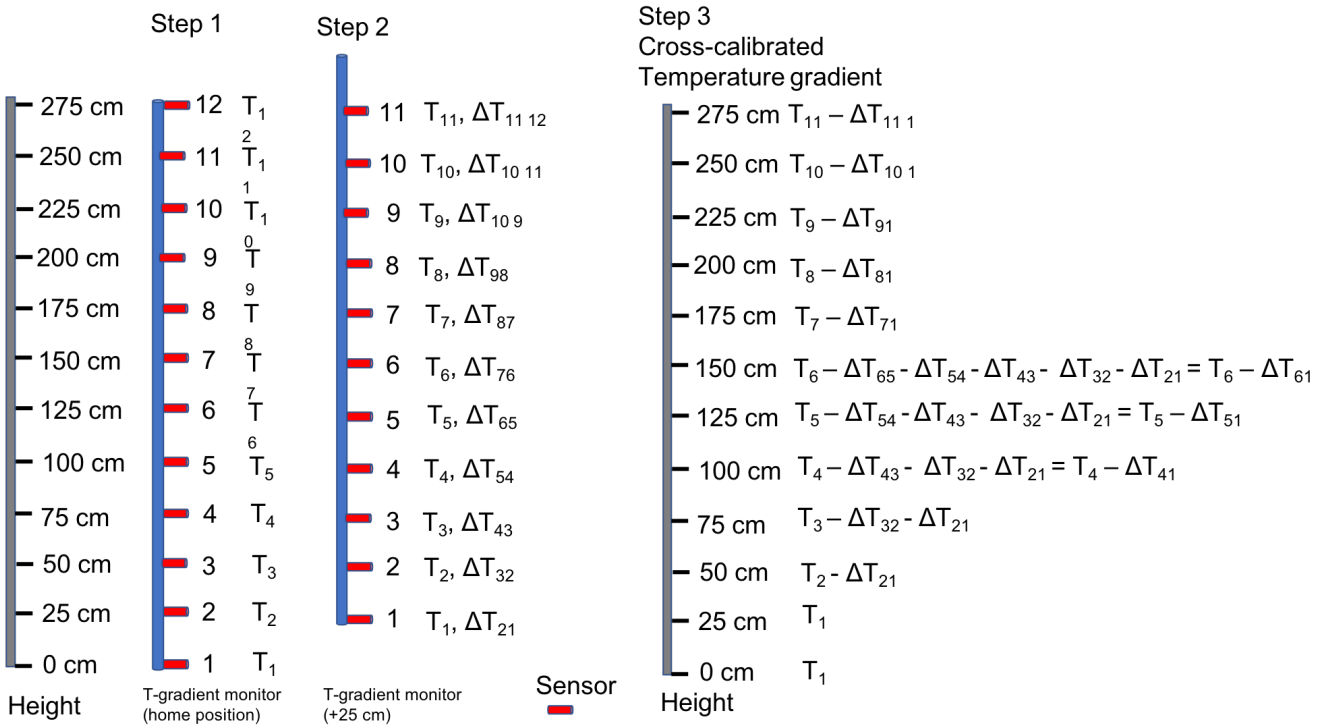


Figure 8.6: In step 1, sensor temperature measurements are taken with the T-gradient monitor in the home position. In step 2, the entire system is moved up 25 cm and another set of temperature readings is taken by all sensors. Then, the offsets between pairs of sensors are calculated for each position. In step 3, offsets are linked together, providing cross-calibration of all sensors, to obtain the entire vertical temperature gradient measurement with respect to a single sensor (number 1 in this case).

the offsets. These measurements are taken with a very stable current source, which ensures high precision of repeated temperature measurements over time. The motion of the dynamic T-monitor is stepper-motor operated, delivering measurements with high spatial resolution.

A total of 72 sensors will be installed with 25 cm spacing, decreased to 10 cm spacing for the top and bottom 1 m of the carrier rod. The vertical displacement of the system is such that every sensor can be moved to the nominal position of at least five other sensors, minimizing the risks associated with sensor failure and allowing for several points of comparison. The total expected motion range of the carrier rod is 1.35 m.

This procedure was tested in ProtoDUNE-SP, where the system was successfully moved up by a maximum of 51 cm, allowing cross-calibration of all sensors (22 sensors with 10.2 cm spacing at top and bottom and 51 cm in the middle).

Figure 8.7 shows the temperature profile after calibration when the recirculation pumps are off. Under these conditions the temperature should be very homogeneous except near the surface. This is indeed what is observed in that figure, demonstrating the reliability of the method.

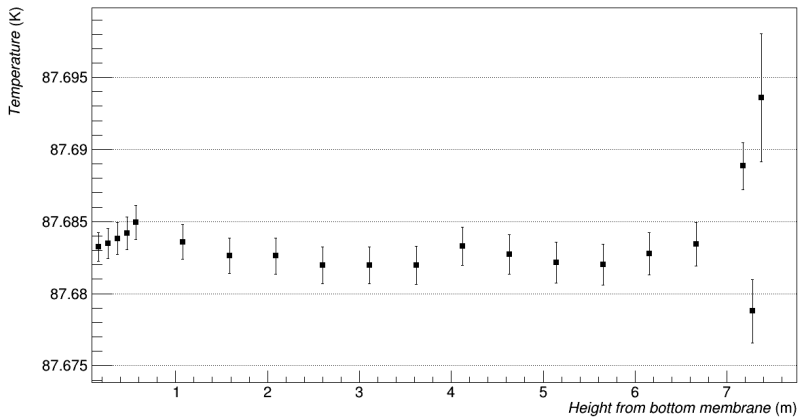


Figure 8.7: Temperature profile as measured by the dynamic T-gradient monitor after cross-calibration, when the recirculation pumps are off. Temperature variation is of the order of 3 mK except close to the top and the gas phase interface, as expected.

A dynamic T-gradient monitor has three parts: a carrier rod on which sensors are mounted; an enclosure above the cryostat housing space that allows the carrier rod to move vertically 1.5 m over its lowest location; and the motion mechanism. The motion mechanism consists of a stepper motor connected through a ferrofluidic dynamic seal to a gear and pinion motion mechanism. The sensors have two pins soldered to a PCB. Two wires are individually soldered to the common soldering pad for each pin. A cutout in the PCB around the sensor allows free flow of argon for more accurate temperature readings. Stepper motors typically have very fine steps that allow highly precise positioning of the sensors. Figure 8.8 shows the overall design of the dynamic T-gradient monitor. The enclosure has two parts connected by a six-cross flange. One side of this flange will be used for signal wires, another will be used as a viewing window, and the two other ports will be spares. Figure 8.9, left shows the PCB mounted on the carrier rod and the sensor mounted on the PCB along with the four point connection to the signal readout wires. Figure 8.9, right shows the stepper motor mounted on the side of the rod enclosure. The motor remains outside the enclosure, at room temperature, as do its power and control cables.

Figure 8.8: A schematic of the dynamic T-gradient monitor.

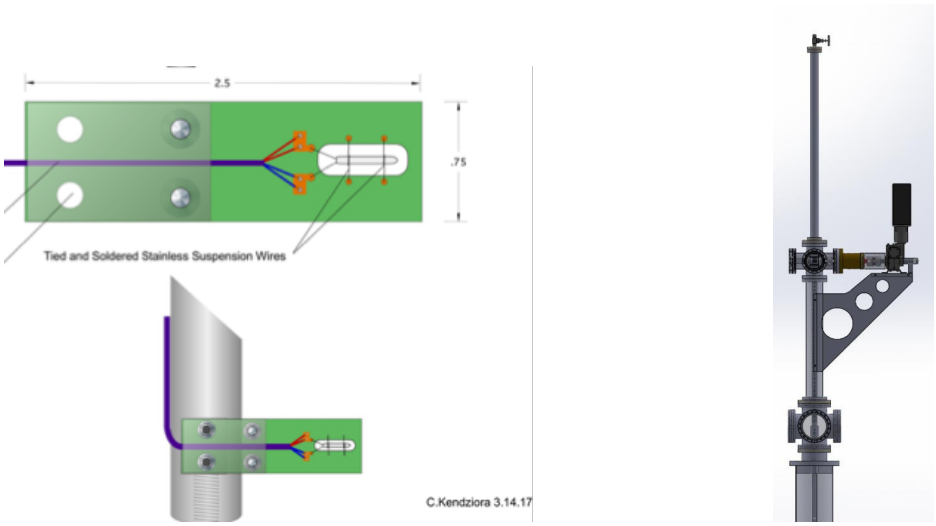


Figure 8.9: Left: Sensor mounted on a PCB board and PCB board mounted on the rod. Right: The driving mechanism of the dynamic T-gradient monitor, consisting of a stepper motor driving the pinion and gear linear motion mechanism.

#### 8.2.1.2 Static T-gradient monitors

Several vertical arrays of high-precision temperature sensors cross-calibrated in the laboratory will be installed behind the APAs. The baseline design assumes six arrays with 48 sensors each. Spacing between sensors is 20 cm at the top and bottom and 40 cm in the middle area. This configuration is similar to the one used in ProtoDUNE-SP but with nearly double the spacing. As shown in Figure 8.10 a configuration with 48 sensors was appropriate in ProtoDUNE-SP, as it should be in the SP module where the expected total gradient is no larger than in ProtoDUNE-SP (see Figure 8.2).

Sensors will be cross-calibrated in the laboratory using a controlled environment and a high-precision readout system, described in Section 8.2.1.5. The accuracy of the calibration for ProtoDUNE-SP was estimated to be 2.6 mK, as shown in Figure 8.11. Preliminary results for the analysis of ProtoDUNE-SP static T-gradient monitor data are shown in Figure 8.10. The temperature profile has been computed using both the laboratory calibration and the so-called "in-situ pump-off calibration," which consists of estimating the offsets between sensors assuming the temperature of LAr in the cryostat is homogeneous when the re-circulation pumps are off (the validity of this method is demonstrated in Section 8.2.1.1). The RMS of the difference between both methods is 4.6 mK, slightly larger than the value quoted above for the accuracy of the laboratory calibration, due to the presence of few outliers (under investigation) and to the imperfect assumption of homogeneous temperature when pumps are off (see Figure 8.7).

Figure 8.12 shows the baseline mechanical design of the static T-gradient monitor. Two strings

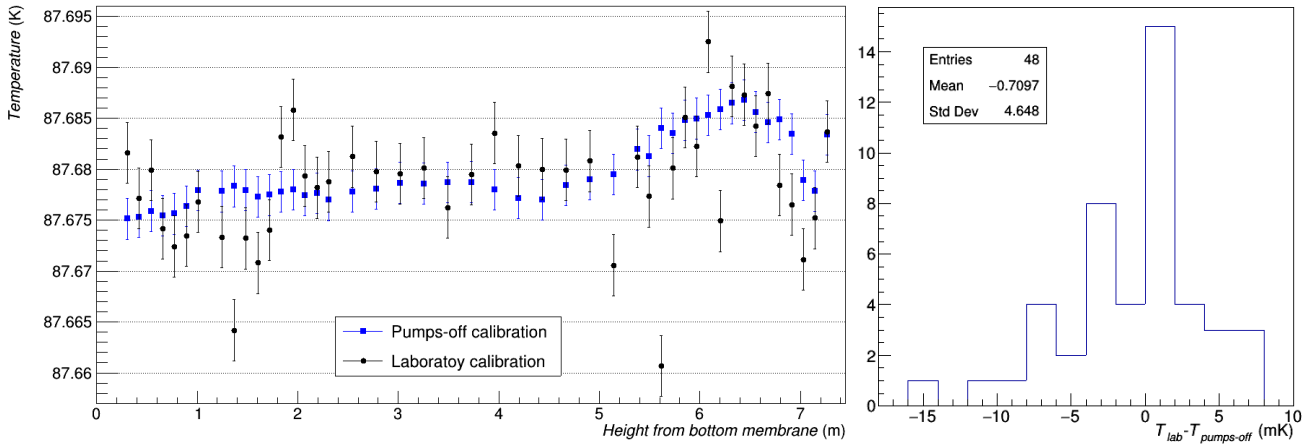


Figure 8.10: Left: Temperature profile as measured by the static T-gradient monitor for two different calibration methods. Right: Distribution of the difference between both methods.

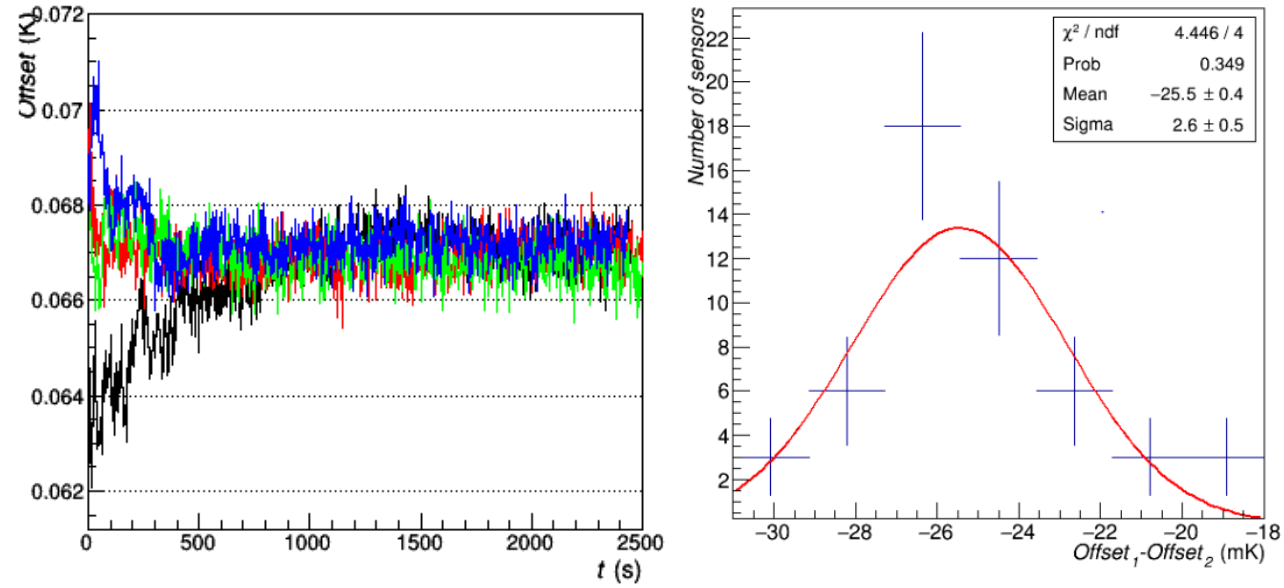


Figure 8.11: Left: Temperature offset between two sensors as a function of time for four independent immersions in LAr. The reproducibility of those sensors, defined as the RMS of the mean offset in the flat region, is $\sim$ 1 mK, The resolution for individual measurements, defined as the RMS of one offset in the flat region, is better than 0.5 mK. Right: Difference between the mean offset obtained with two independent calibration methods for the 51 calibrated sensors. The standard deviation of this distribution is interpreted as precision of the calibration.

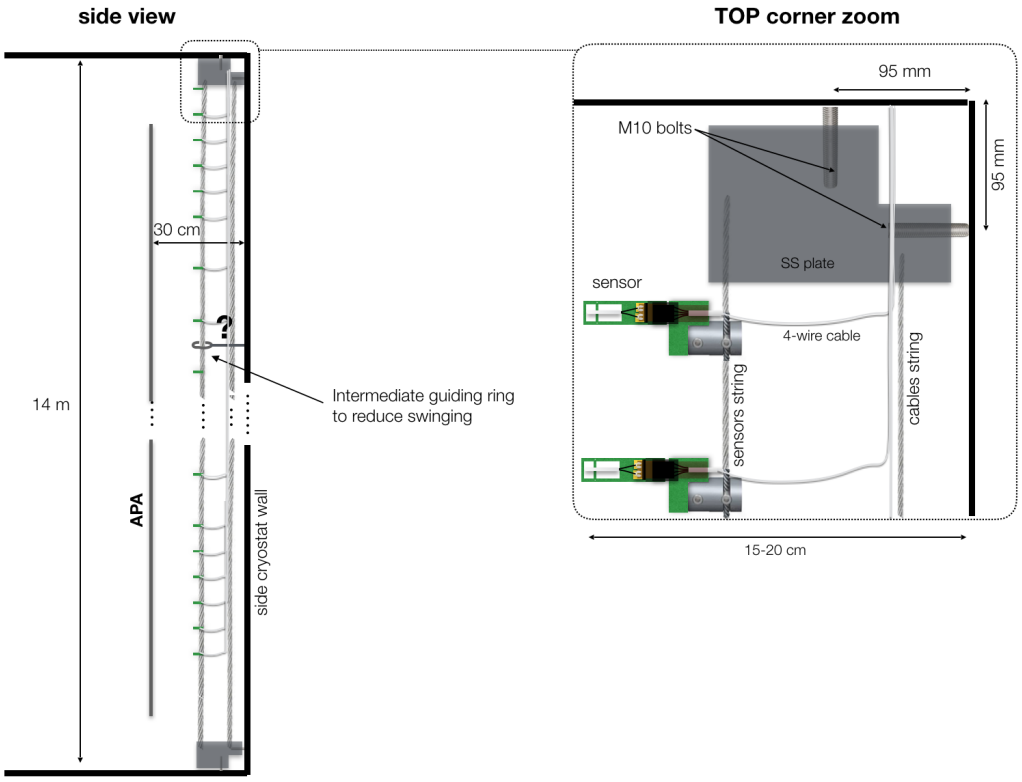


Figure 8.12: Conceptual design of the static T-gradient monitor.

(stainless steel or carbon fibre) are anchored at the top and bottom corners of the cryostat using the available M10 bolts (see Figure 8.13, left). One string routes the cables while the other supports the temperature sensors. Given the height of the cryostat, an intermediate anchoring point to reduce swinging is under consideration. A prototype is being built at IFIC, Spain, where the full system will be mounted using two dummy cryostat corners.

Figure 8.13 (right) shows the baseline design of the ($52 \times 15\,\mathrm{mm}^2$) PCB support for temperature sensors with an IDC-4 male connector. A narrower connector (with two rows of two pins each) is being studied. This alternative design would reduce the width of the PCB assembly and allow more sensors to be calibrated simultaneously. Each four-wire cable from the sensor to the flange will have an IDC-4 female connector on the sensor end; the flange end of the cable will be soldered or crimped to the appropriate connector, whose type and number of pins depend on the final design of the DSS ports that will be used to extract the cables. SUBD-25 connectors were used in ProtoDUNE-SP.

#### 8.2.1.3 Individual Temperature Sensors

T-gradient monitors will be complemented by a coarser 2D array (every 5 m) of precision sensors at the top and bottom of the detector module, as shown in Figure 8.5. Following the ProtoDUNE-SP design, bottom sensors will use the cryogenic pipes as a support structure, while top sensors will be anchored to the GPs. Although sensors at the top will have a similar distribution to those at

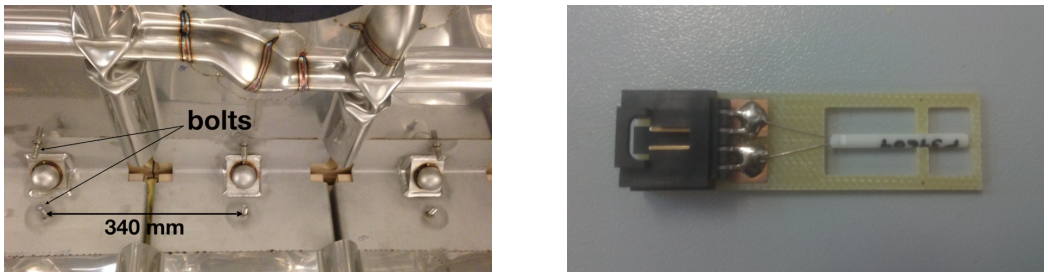


Figure 8.13: Left: bolts at the bottom corner of the cryostat. Right: Lakeshore PT102 sensor mounted on a PCB with an IDC-4 connector.

the bottom, suitable anchoring points at the top and bottom will differ.

As in ProtoDUNE-SP, another set of standard sensors will be evenly distributed and epoxied to the bottom membrane. They will detect the presence of LAr when cryostat filling starts. Finally, two vertical arrays of standard sensors will be epoxied to the lateral walls in two opposite vertical corners, with a spacing of 102 cm (every three corrugations), to monitor the cryostat membrane temperature during the cool-down and filling processes.

Whereas in ProtoDUNE-SP cables were routed individually (without touching neighboring cables or any metallic elements) to prevent grounding loops in case the outer Teflon jacket broke, such a failure has been proved to be very unlikely. Thus, in the detector modules, cables will be routed in bundles, simplifying the design enormously. As Figure 8.5 shows, up to 20 sensors will use the same DSS port, large enough for a cable bundle 16 mm in diameter.

Cable bundles of several sizes will be configured using custom made Teflon pieces that will be anchored to different cryostat and detector elements to route cables from sensors to DSS ports. For sensors at the bottom (on pipes and floor), cables will be routed towards the cryostat bottom horizontal corner using stainless steel split clamps anchored to pipes (successfully prototyped in ProtoDUNE-SP), and from there, to the top of the cryostat using vertical strings (as with static T-gradient monitors). For sensors on the top GPs, cables bundles will be routed to the corresponding DSS port using Teflon supports attached to both the FR-4 threaded rods in the union between two GP modules and to the DSS I-beams (both successfully prototyped in ProtoDUNE-SP). Sensors on the walls will use bolts in the vertical corners for cable routing.

For all individual sensors, PCB sensor support, cables, and connection to the flanges will be the same as for the T-gradient monitors.

#### 8.2.1.4 Analysis of temperature data in ProtoDUNE-SP

Temperature data from ProtoDUNE-SP has been recorded since LAr filling in August 2018. The analysis of this data and the comparison with CFD simulations is actively underway, but interesting preliminary results are available and are described below. Figure 8.14 shows the distribution of temperature sensors in the ProtoDUNE-SP cryostat.

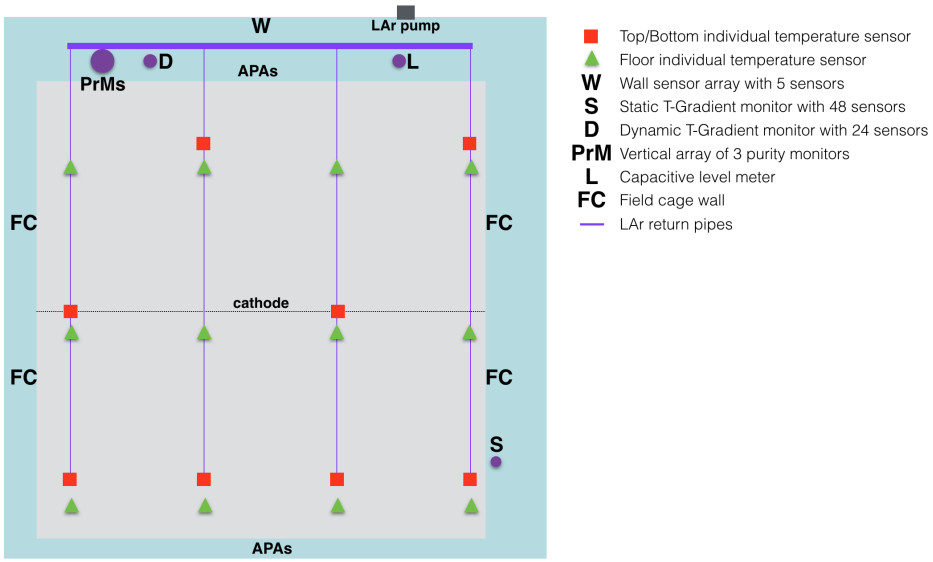


Figure 8.14: Distribution of temperature sensors in the ProtoDUNE-SP cryostat. Notice that four of the bottom sensors are located right above the LAr inlets. Purity monitors and level meters are also indicated.

All precision temperature sensors (for the static and dynamic T-gradient monitors, and the 2D arrays at top and bottom) were calibrated in the laboratory prior to installation, as described in Section 8.2.1.2. However, since the calibration method was still under development when those sensors were installed, this calibration was only satisfactory (2.6 mK precision) for the static T-gradient monitor, for which the sensors were calibrated last and plugged in just few days prior to installation in the cryostat. In Section 8.2.1.2, an additional calibration method, the so-called "pumps-off calibration," is described and the agreement with the laboratory calibration was demonstrated (see Figure 8.10). Since this is the only reliable calibration for individual sensors, this method is used for the data analysis presented in this section, for all sensors except for the dynamic T-gradient monitor, for which the calibration based on the movable system is more precise (see Section 8.2.1.1).

Figure 8.15 shows the vertical temperature profiles as measured by the dynamic and static T-gradient monitors during a 10 minute period in May 2019. The stability of these profiles has been carefully studied: the relative variation between any two sensors on the same profiler remained below 3 mK during the entire data taking period, demonstrating that the shape of the profiles is nearly constant in time. In Figure 8.15 it is clear that the shapes of the two profiles are similar, with a bump at 6.2 m, but the magnitude of variation of the static profile almost doubles compared to the dynamic profile. This effect is attributed to the fact that the dynamic T-gradient monitor is in the path of the LAr flow, which makes the temperature more uniform, while the static profiler is on the side.

We can use temperature measurements by the bottom sensor grid to connect the two different regions covered by the T-gradient monitors. Figure 8.16 shows the temperature difference between bottom sensors and the second sensor of the static T-gradient monitor, 40 cm from the floor, which is used as a reference. Also shown in the figure is the dynamic T-gradient monitor's third sensor, located at a similar height. Three different periods are shown in the figure: two periods with pumps-on and one period with pumps-off. It is observed that when the pumps are working, the

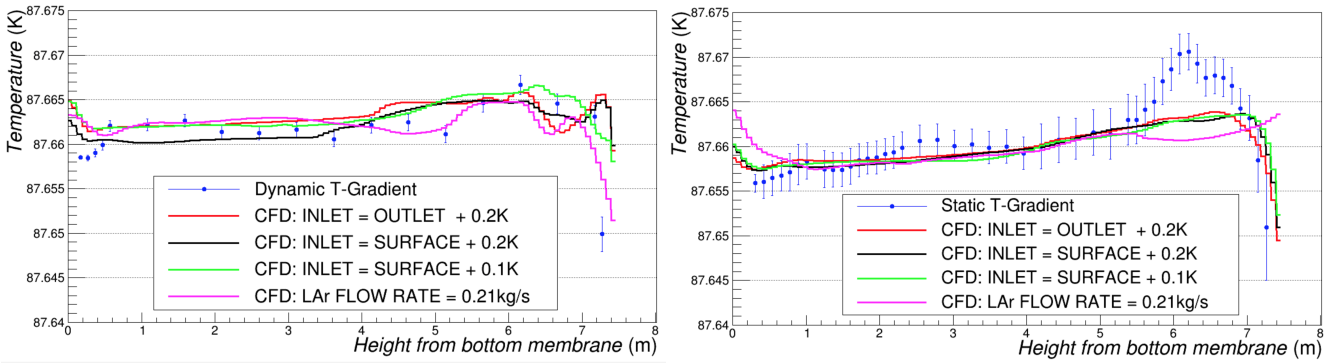


Figure 8.15: Temperature profiles measured by the T-gradient monitors and comparison to the CFD model with different boundary conditions. Left: dynamic T-gradient monitor; Right: Static T-gradient monitor.

temperature decreases towards the LAr pump, and is higher in the sensors below the cathode. The horizontal gradient observed in this situation is of the order of 20 mK – larger than the vertical gradient. When the pumps are off the horizontal gradient decreases, although a residual gradient of 5 mK is observed. This gradient is attributed to the inertia of the liquid once the pumps are switched off: it takes more than one day to recover the horizontal homogeneity.

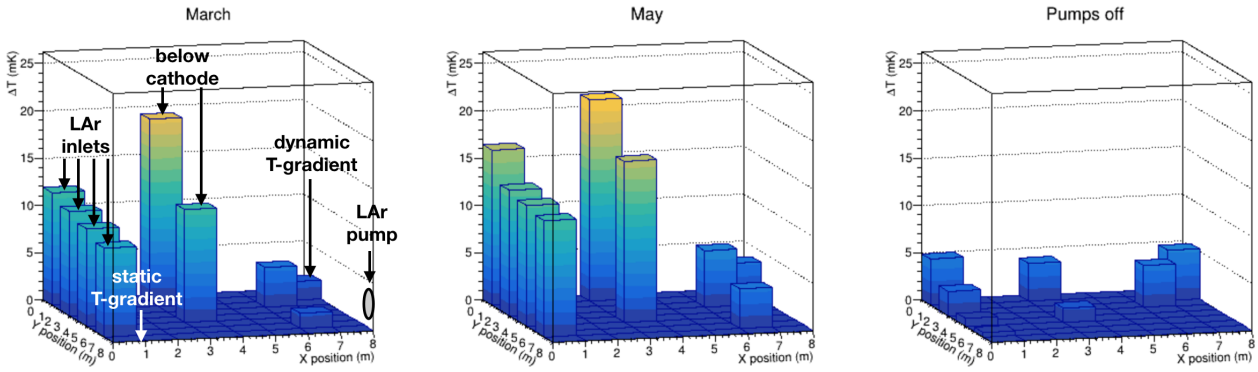


Figure 8.16: Temperature difference between bottom sensors at 40 cm from the floor and static T-gradient sensor at same height. The third dynamic T-gradient sensor, at the same height, is also shown. Two pumps-on periods (left and middle panels) and one pump-off period (right panel) are shown.

CFD simulations have been produced using different inputs. We have identified two parameters as potential drivers of the convection regime: (1) the incoming LAr flow rate, and (2) the incoming LAr temperature. Figure 8.15 shows the result of varying these parameters. The CFD model reasonably predicts the main features of the data, but some details still need to be understood, in particular the bump at 6.2 m and the lower measured temperature at the bottom. It is worth noting that the simulation depends minimally on the LAr temperature while the flow rate has more impact, especially in the regions where discrepancies are larger. All simulations use the nominal LAr flow rate, 0.42 kg/s, except the one explicitly indicated in the plots that uses half that rate. More simulations with other LAr flow rates are still in progress.

The CFD reassuringly predicts a reasonable response for more than one set of initial conditions. It

is still important to measure the instrumentation response to help establish the validity of the CFD model. We did not run tests with differing initial conditions during the beam run because even controlled changes of the cryostat environment could have undesirable effects. However, recently we ran dedicated tests to validate the CFD under various deliberate changes of the cryostat. These additional tests included pump and recirculation manipulations (such as pump on-off, change of pumping speed, and bypassing of filtration), and changing the cryostat pressure set point to a higher (or lower) value[7] to induce changes in the pressure for a specified time while monitoring the instrumentation. Any change in pressure could change the temperatures everywhere in the cryostat. Studying the rate of this change, as detected at various heights in the cryostat, might provide interesting constraints on the CFD model.

#### 8.2.1.4.1 Comparison of calibration methods

Three different calibration methods have been described above: a laboratory calibration prior to installation, the "pumps off" calibration, and the movable system calibration. The underlying assumption is that reliable temperature monitoring at the few mK level is desirable during the entire lifetime of the experiment, both to guarantee the correct functioning of the cryogenics system and to compute offline corrections based on temperature measurements and CFD simulations. This is only possible if an in situ calibration method is available, since relative calibration between sensors is expected to diverge with time. Two in situ methods have been used. The pumps-off calibration method is very powerful since it is the only way of cross-calibrating all sensors in the cryostat at any point in time. However, it relies on the assumption that the temperature is uniform when the recirculation pumps are off. The validity of this assumption has to be bench-marked with real data, and this is done in ProtoDUNE-SP using the calibration based on the movable system (see Figure 8.7). The movable system calibration method is the most precise and the one that sustains all other methods, providing a reliable reference during the entire lifetime of the experiment. This method is even more crucial for the FD. Indeed, recirculation pumps will be located on one side of the cryostat, very far (almost 60 m) from some regions of the LAr volume, where the inertia will be more pronounced and the homogeneous temperature assumption becomes less valid.

### 8.2.1.5 Readout system for thermometers

A high-precision and very stable system is required to achieve a readout level of $< 5$ mK. The proposed readout system was used in ProtoDUNE-SP and relies on a variant of an existing mass PT100 temperature readout system developed at European Organization for Nuclear Research (CERN) for an LHC experiment; it has already been tested and validated in ProtoDUNE-SP. The system has an electronic circuit that includes

- a precise and accurate current source[8] for the excitation of the temperature sensors measured

[7] The HV was ramped down for this exercise because dropping the pressure too fast might provoke boiling of the LAr near the surface.

[8] The actual current delivered is monitored with high-precision resistors such that the effect of ambient temperature

using the four-wires method,

- a multiplexing circuit connecting the temperature sensor signals and forwarding the selected signal to a single line, and
- a readout system with a high-accuracy voltage signal readout module[9] with 24 bit resolution over a 1 V range.

This readout system also drives the multiplexing circuit and calculates temperature values. The CompactRIO device is connected to the detector Ethernet network, sending temperature values to the DCS software through a standard OPC-UA driver.

The current mode of operation averages more than 2000 samples taken every second for each sensor. Figure 8.11 shows the system has a resolution higher than 1 mK, the RMS of one of the offsets in the stable region.

### 8.2.2 Purity Monitors

A fundamental requirement of a liquid argon time-projection chamber (LArTPC) is that ionization electrons drift over long distances in the liquid. Part of the charge is inevitably lost due to electronegative impurities in the liquid. To keep this loss to a minimum, monitoring impurities and purifying the LAr during operation is essential.

A purity monitor is a small ionization chamber used to infer independently the effective free electron lifetime in the LArTPC. It illuminates a cathode with UV light to generate a known electron current, then collects the drifted current at an anode a known distance away. Attenuation of the current is related to the electron lifetime. Electron loss can be parameterized as $N(t) = N(0)e^{-t/\tau}$, where $N(0)$ is the number of electrons generated by ionization, $N(t)$ is the number of electrons after drift time $t$, and $\tau$ is the electron lifetime.

For the SP module, the drift distance is 3.5 m, and the E field is $500\,\mathrm{V}\cdot\mathrm{cm}^{-1}$. Given the drift velocity of approximately $1.5\,\mathrm{mm}\cdot\mu\mathrm{s}^{-1}$ in this field, the time to go from cathode to anode is roughly $\sim$2.4 ms [103]. The LArTPC signal attenuation, $[N(0) - N(t)]/N(0)$, must remain less than 20 % over the entire drift distance [163]. The corresponding electron lifetime is $2.4\,\mathrm{ms}/[-\ln(0.8)] \simeq 11\,\mathrm{ms}$.

Residual gas analyzers can be used to monitor the gas in the ullage of the tank and would be an obvious choice for analyzing argon gas. Unfortunately, suitable and commercially available mass spectrometers have a detection limit of $\sim$10 parts per billion (ppb), whereas DUNE requires a sensitivity of parts per trillion (ppt). Therefore, specially constructed and distributed purity monitors will measure LAr purity in all phases of operation. These measurements, along with an accurate CFD model, enable the determination of purity at all positions throughout the detector module.

can be disentangled.

[9] National Instrument CompactRIO™ device with a signal readout NI9238™ module.

Purity monitors are placed inside the cryostat but outside of the TPC. They are also placed within the recirculation system outside the cryostat, both in front of and behind the filtration system. Continuous monitoring of the LAr supply lines to the detector module provides a strong line of defense against contamination from sources both in the LAr volume and from components in the recirculation system. Similarly, gas analyzers (described in Section 8.2.5) protect against contaminated gas.

Furthermore, using several purity monitors to measure lifetime with high precision at carefully chosen points provides key input, e.g., vertical gradients in impurity concentrations, for CFD models of the detector module.

Purity monitors were deployed in previous LArTPC experiments, e.g., ICARUS, MicroBooNE, and the 35 ton prototype. During the first run of the 35 ton prototype, two of the four purity monitors stopped working during cool-down, and a third operated intermittently. We later found that this was due to poor electrical contacts between the resistor chain and the purity monitor. A new design was implemented and successfully tested in the second run.

ProtoDUNE-SP and ProtoDUNE-DP use purity monitors to measure electron lifetime at different heights, and they use a similar design.

Figure 8.17 shows the assembly of the ProtoDUNE-SP purity monitors. The design reflects improvements to ensure electrical connectivity and improve signals. ProtoDUNE-SP uses a string of purity monitors connected with stainless steel tubes to protect the optical fibers.

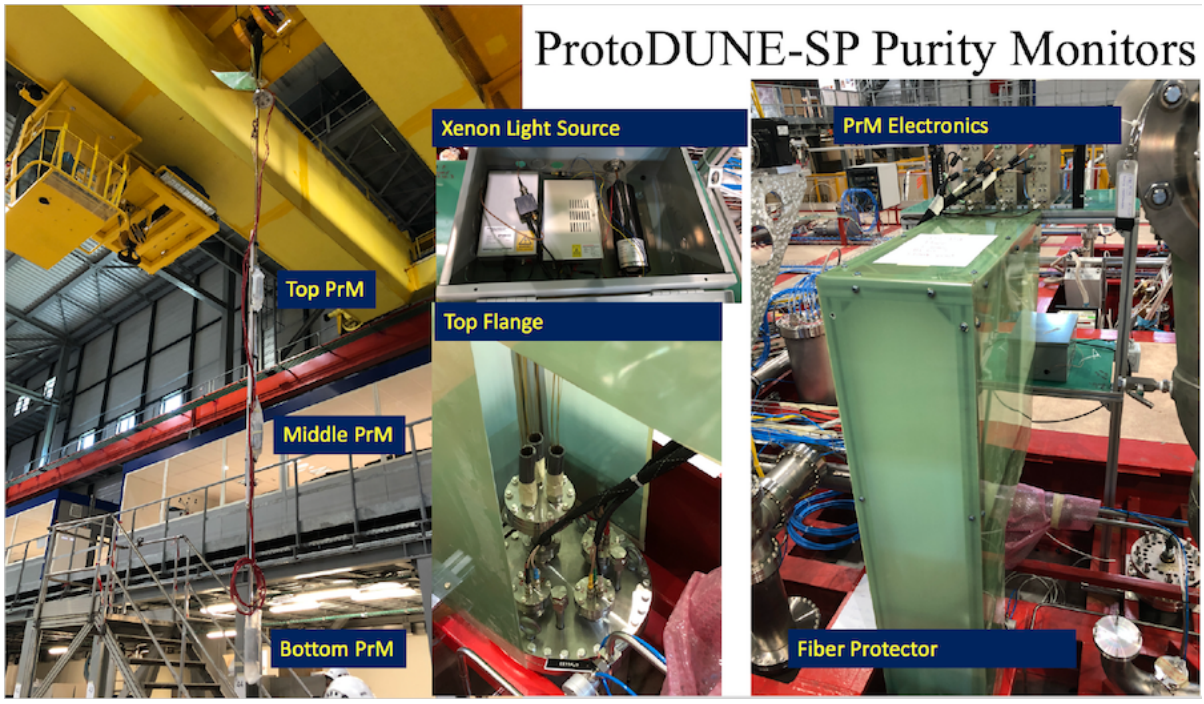


Figure 8.17: The ProtoDUNE-SP purity monitoring system

ProtoDUNE-SP implements three purity monitors. The purity monitors continuously monitored LAr purity during all commissioning, beam test and operation periods of ProtoDUNE-SP. Figure 8.18 shows the ProtoDUNE-SP data taken using its three purity monitors from commissioning

of ProtoDUNE-SP starting in September 2018, through the entire beam running period, to July 2019.

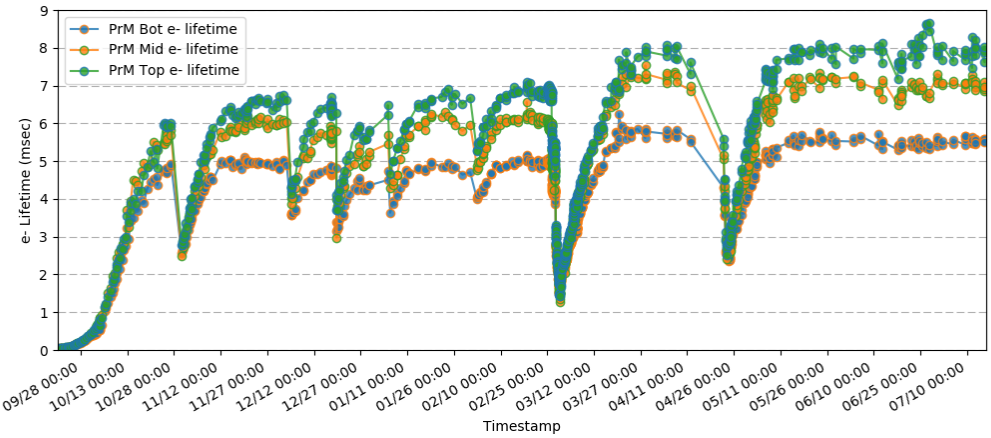


Figure 8.18: The electron lifetimes measured by three purity monitors in ProtoDUNE-SP as a function of time, September 2018 through July 2019. The purity is low prior to start of circulation in October. Reasons for later dips include recirculation studies and recirculation pump stoppages.

Although ProtoDUNE-SP receives ample cosmic ray data to perform electron lifetime measurements, the purity monitor system was found to be essential for providing quick, reliable real-time monitoring of purity in the detector and to catch purity-related changes in time due to LAr recirculation issues. Each purity monitor electron lifetime measurement is based on purity monitor anode-to-cathode signal ratios from 200 UV flashes within 40 seconds at the same location. The statistical error on this lifetime measurement is less than 0.03 ms when the purity is 6 ms.

The purity monitor system at ProtoDUNE-SP measured electron lifetime every hour during commissioning and daily during the beam test. During this time, it alerted the experiment to problems several times. The first time was for filter saturation during LAr filling, and the others were for recirculation pump stoppages, false alarms, and problems from the cryostat-level gauges. The dips in Figure 8.18 show these sudden changes in purity caught by purity monitors. Given the high sensitivity, the ProtoDUNE-SP purity monitors were immediately able to alert the experiment to the purity drops, preventing situations which otherwise would have continued unnoticed for some time, with potentially serious consequences for the ability to take any data.

During the commissioning and beam test of ProtoDUNE-SP, the purity monitors operated with different high voltages to change electron drift time, ranging from 150 µs to 3 ms. This allowed the ProtoDUNE-SP purity monitors to measure electron lifetime from 35 µs to about 10 ms with high precision, a dynamic range greater than 300. This measurement was also valuable for the ProtoDUNE-SP lifetime calibration. Because purity monitors have much smaller drift volumes than the TPC, they are less affected by the space charge caused by cosmic rays.

A similar operation plan is planned for the SP module, with modifications to accommodate the relative positions of the instrumentation port and the purity monitor system, and the different geometric relationships between the TPC and cryostat.

#### 8.2.2.1 Purity Monitor Design

The SP module baseline purity monitor design follows that of the ICARUS experiment (Figure 8.19)[164]. It consists of a double-gridded ion chamber immersed in the LAr volume with four parallel, circular electrodes, a disk holding a photocathode, two grid rings (anode and cathode), and an anode disk. The cathode grid is held at ground potential. The cathode, anode grid, and anode each hold separate bias voltages and are electrically accessible via modified vacuum-grade HV feedthroughs. The anode grid and the field-shaping rings are connected to the cathode grid by an internal chain of 50 MΩ resistors to ensure the uniformity of the E fields in the drift regions. A stainless mesh cylinder is used as a Faraday cage to isolate the purity monitor from external electrostatic background.

The purity monitor measures the electron drift lifetime between its anode and cathode. The purity monitor's UV-illuminated photocathode generates the electrons via the photoelectric effect. Because the electron lifetime in LAr is inversely proportional to the electronegative impurity concentration, the fraction of electrons generated at the cathode that arrives at the anode ($Q_A/Q_C$) after the electron drift time $t$ gives a measure of the electron lifetime $\tau$: $Q_A/Q_C \sim e^{-t/\tau}$.

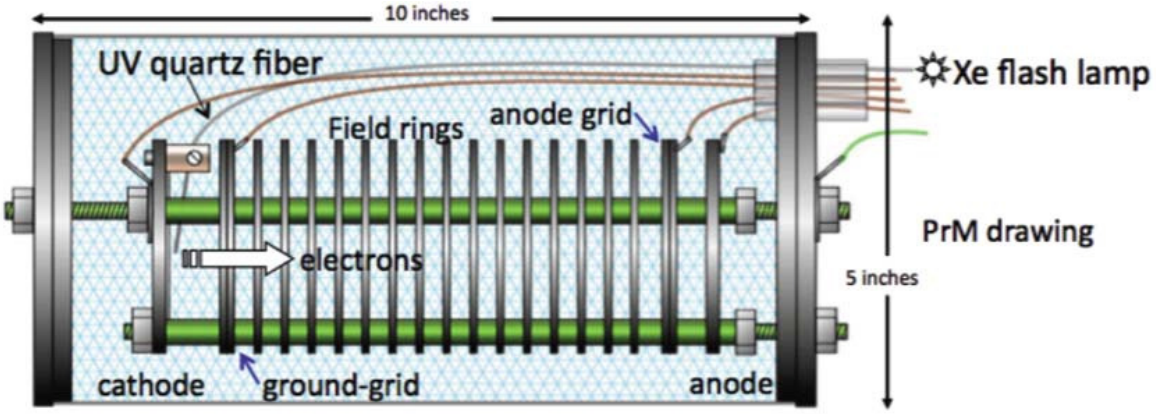


Figure 8.19: Schematic diagram of the basic purity monitor design [164].

Once the electron lifetime becomes much larger than the drift time $t$ the purity monitor reaches its sensitivity limit. For $\tau >> t$, the anode-to-cathode charge ratio becomes $\sim$1. Because the drift time is inversely proportional to the E field, in principle, lowering the field should make it possible to measure lifetimes of any length, regardless of the length of the purity monitor. On the other hand, increasing the voltage will shorten the drift time, allowing measurement of a short lifetime when purity is low.

The electron lifetime of the purest commercial LAr, after the first filtering and during the filling process, is typically higher than 40 µs. However, when the filter starts to saturate, the lifetime decreases to less than 30 µs. To reduce the energy loss due to impurities, the SP module requires an electron lifetime greater than 3 ms.

Varying the operational HV on the anode from 250 V to 4000 V in the ProtoDUNE-SP's 24 cm (9.5 inch) long purity monitor allowed us to make the 35 µs to 10 ms electron lifetime measurements. Purity monitors with different lengths (drift distances) are needed to extend the measurable range

to below 35 µs and above 10 ms.

The photocathode that produces the photoelectrons is an aluminum plate coated first with 50 Å of titanium followed by 1000 Å of gold, and is attached to the cathode disk. A xenon flash lamp is the light source in the baseline design, although a more reliable and possibly submersible light source, perhaps LED-driven, could replace this in the future. The UV output of the lamp is quite good, approximately $\lambda = 225$ nm, which corresponds closely to the work function of gold (4.9 eV to 5.1 eV). Several UV quartz fibers carry the xenon UV light into the cryostat to illuminate the photocathode. Another quartz fiber delivers the light into a properly biased photodiode outside the cryostat to provide the trigger signal when the lamp flashes.

#### 8.2.2.2 Electronics, DAQ, and Slow Controls Interfacing

The purity monitor electronics and DAQ system consist of front-end (FE) electronics, waveform digitizers, and a DAQ PC. Figure 8.20 illustrates the system.

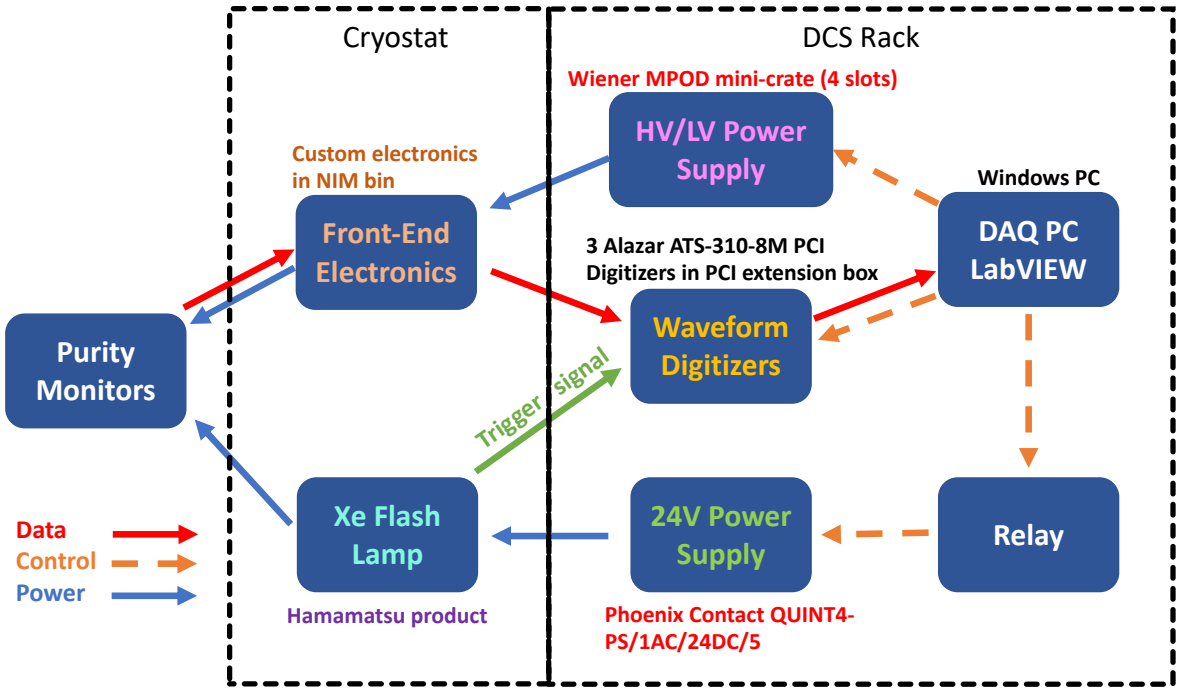


Figure 8.20: Block diagram of the purity monitor system.

The baseline design of the FE electronics follows that used in the 35 ton prototype, Liquid Argon Purity Demonstrator (LAPD), and MicroBooNE. The cathode and anode signals are fed into two charge amplifiers contained within the purity monitor electronics module. This electronics module includes a HV filter circuit and an amplifier circuit, both shielded by copper plates, to allow the signal and HV to be carried on the same cable and decoupled inside the purity monitor electronics module. A waveform digitizer that interfaces with a DAQ PC records the amplified anode and cathode outputs. The signal and HV cable shields connect to the grounding points of the cryostat and are separated from the electronic ground with a resistor and a capacitor connected in

parallel, mitigating ground loops between the cryostat and the electronics racks. Amplified output is transmitted to an AlazarTech ATS310 waveform digitizer[10] containing two input channels, each with 12 bit resolution. Each channel can sample a signal at a rate of $20\,\mathrm{MS}\cdot\mathrm{s}^{-1}$ to $1\,\mathrm{kS}\cdot\mathrm{s}^{-1}$ and store up to 8 MS in memory. One digitizer is used for each purity monitor, and each digitizer interfaces with the DAQ PC across the PCI bus.

A custom LabVIEW[11] application running on the DAQ PC has two functions: it controls the waveform digitizers and the power supplies, and it monitors the signals and key parameters. The application configures the digitizers to set the sampling rate, the number of waveforms to be stored in memory, the pre-trigger data, and a trigger mode. A signal from a photodiode triggered by the xenon flash lamp is fed directly into the digitizer as an external trigger to initiate data acquisition. LabVIEW automatically turns on the xenon flash lamp by powering a relay when data taking begins and then turns it off when finished. The waveforms stored in the digitizers are transferred to the DAQ PC and used to obtain averaged waveforms to reduce the electronic noise in them.

The baseline is estimated by averaging the waveform samples prior to the trigger. This baseline is subtracted from the waveforms prior to calculating peak voltages of the cathode and anode signals. The application performs these processes in real time. The application continuously displays the waveforms and important parameters like measured electron lifetime, peak voltages, and drift time in the purity monitors, and shows the variation in these parameters over time, thus pointing out effects that might otherwise be missed. Instead of storing the measured parameters, the waveforms and the digitizer configurations are recorded in binary form for offline analysis. HV modules[12] in a WIENER MPOD mini crate[13] supply negative voltages to the cathode and positive voltages to the anode. The LabVIEW application controls and monitors the HV systems through an Ethernet interface.

The xenon flash lamp and the FE electronics are installed close to the purity monitor flange, to reduce light loss through the optical fiber and prevent signal loss. Other pieces of equipment that distribute power to these items and collect data from the electronics are mounted in a rack separate from the cryostat. The slow control system communicates with the purity monitor DAQ software and controls the HV and LV power supplies of the purity monitor system. The optical fiber must be placed within 0.5 mm of the photocathode for efficient photoelectron extraction, so little interference with the photon detection system (PD system) is expected. The purity monitors could induce noise in the TPC electronics, in particular via the current surge through a xenon lamp when it is flashed. This source of noise can be controlled by placing the lamp inside its own Faraday cage with proper grounding and shielding. At ProtoDUNE-SP, after careful checks of the grounding, this noise has remained well below the noise generated by other sources.

In the SP module we can make use of triggering to prevent any potential noise from the purity monitor's flash lamp from affecting TPC and PD system signals. The LArTPC trigger rate is a few hertz, and each trigger window is one or a few milliseconds. The pulse from a flash lamp is very short (a microsecond or so, much shorter than the gaps between LArTPC trigger windows). Thus, a LArTPC trigger signal may be sent to a programmable pulse generator, which generates

[10] AlazarTech ATS310™ - 12 bit, 20 MS/s, https://www.alazartech.com/Product/ATS310.
[11] National Instruments, LabVIEW™, http://www.ni.com/en-us.html
[12] iseg Spezialelektronik GmbH™ high voltage supply systems, https://iseg-hv.com/en.
[13] W-IE-NE-R MPOD™ Universal Low and High Voltage Power Supply System, http://www.wiener-d.com/.

a trigger pulse that does not overlap with LArTPC trigger windows. This trigger pulse is then sent to the external trigger port on the flash lamp HV controller so that the lamp flashes between LArTPC trigger windows. In this way, the electronic and light noises from the flash lamp do not affect data taking at all.

#### 8.2.2.3 Production and Assembly

The CISC consortium will produce the individual purity monitors, test them in a test stand, and confirm that each monitor operates at the required level before assembling them into the strings of three monitors each that will be mounted in the SP module cryostat using support tubes. The assembly process will follow the methodology developed for ProtoDUNE.

A short version of the string with all purity monitors will be tested at the CITF. The full string will be assembled and shipped to South Dakota. A vacuum test in a long vacuum tube will be performed on-site before inserting the full assembly into the SP module cryostat.

### 8.2.3 Liquid Level Meters

The goals for the LAr level monitoring system are basic level sensing when filling, and precise level sensing during static operations.

Filling the cryostat with LAr will take several months. During this operation several systems will be use to monitor the LAr level. The first 5.5 m will be covered by cameras and by the vertical arrays of resistance temperature detectors (RTDs) at known heights, since temperature will change drastically when the cold liquid reaches each RTD. Once the liquid reaches the level of the cryogenics pipes going out of the cryostat, the differential pressure between that point and the bottom of the cryostat can be converted to depth using the known density of LAr. Fine tuning of the final LAr level will be done using several capacitive level meters at the top of the cryostat.

During operation, liquid level monitoring has two purposes: the LBNF cryogenics system uses monitoring to tune the LAr flow, and DUNE uses monitoring to guarantee that the top GPs are always submerged at least 20 cm below the LAr surface to mitigate the risk of dielectric breakdown. This was the value used for the HV interlock in ProtoDUNE-SP.

The LAr flow is tuned using two differential pressure level meters, installed as part of the cryogenics system, one on each side of the detector module. They have a precision of 0.1 %, which corresponds to 14 mm at thenominal LAr surface. Cryogenic pressure sensors will be purchased from commercial sources. Installation methods and positions will be determined as part of the cryogenics internal piping plan.

For HV integrity, multiple 4 m long capacitive level sensors (with a precision of less than 5 mm) will be deployed along the top of the fluid for use during stable operations, and checked against each other. One capacitive level sensor at each of the four corners of the cryostat will provide

sufficient redundancy to ensure that no single point of failure compromises the measurement.

Figure 8.21 shows the evolution of the ProtoDUNE-SP LAr level over two months as measured by the differential pressure and capacitive level meters.

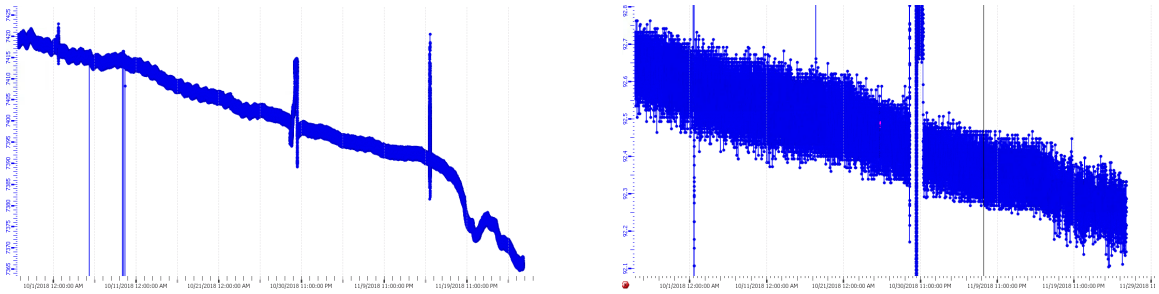

Figure 8.21: Evolution of the ProtoDUNE-SP LAr level over two months. Left: Measured by the capacitive level meter. Right: Measured by the differential pressure level meter. The units in the vertical axis are percentages of the cryostat height (7878 mm).

ProtoDUNE-SP uses the same design for differential pressure level meters as the SP module. In the case of capacitive level meters, ProtoDUNE-SP is using commercially bought 1.5 m long level meters while ProtoDUNE-DP is using 4 m long level meters that are custom-built by CERN. We plan to use the longer capacitive level meters custom-built by CERN for both SP and DP modules.

### 8.2.4 Pressure Meters

The absolute temperature in the liquid varies with the pressure in the argon gas in the ullage of the cryostat, therefore, precise measurements of pressure inside the cryostat allow for a better understanding of temperature gradients and CFD simulations. In ProtoDUNE-SP, pressure values were also used to understand the strain gauge signals installed in the cryostat frame.

Standard industrial pressure sensors can be used to measure the pressure of the argon gas. For the DUNE FD, the plan is to follow the same design and configuration used in ProtoDUNE-SP. ProtoDUNE uses two types of pressure sensors and a pressure switch,

- a relative pressure sensor (range: 0-400 mbar, precision: 0.01 mbar),
- an absolute pressure sensor (range: 0-1600 mbar, precision: 0.05 mbar), and
- a mechanical relative pressure switch adjustable from 50 to 250 mbar.

Both sensors and the pressure switch are installed in a dedicated flange as shown in Figure 8.22 and are connected directly to a slow controls system PLC circuit. Dedicated analog inputs are used to read the current values (4 mA to 20 mA) which are then converted to pressure according to the sensors range. Given the much larger size of the DUNE detector modules, the system described above will be doubled for redundancy: two flanges in opposite cryostat sides will be instrumented with three sensors each.

Further, relative and absolute pressure sensors (with comparatively lower precision) are installed

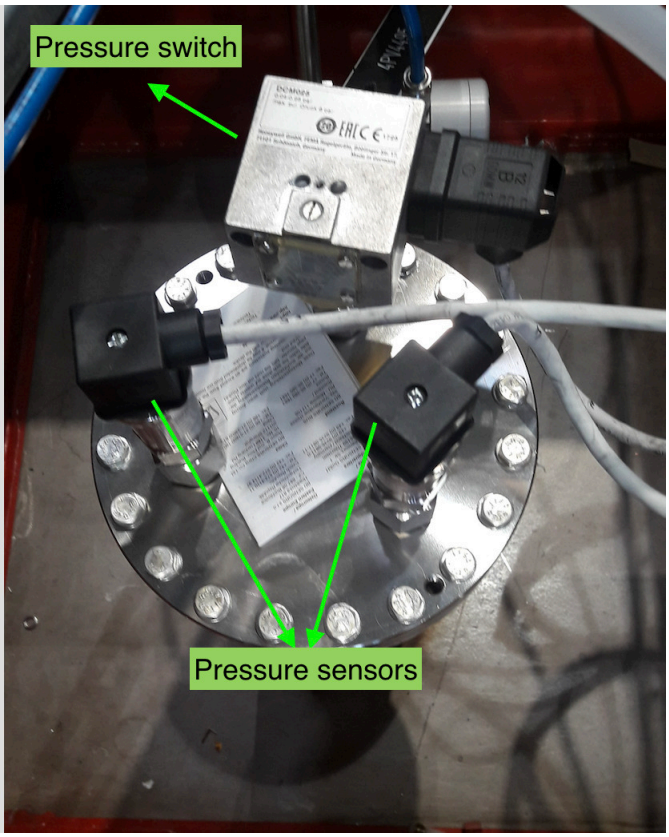


Figure 8.22: Photograph of the pressure sensors installed on a flange in ProtoDUNE-SP.

by LBNF that are also recorded by the slow controls system. The availability of two types of sensors from LBNF and CISC provides redundancy, independent measurements, and cross checks.

### 8.2.5 Gas Analyzers

Gas analyzers are commercially produced modules that measure trace quantities of specific gases contained within a stream of carrier gas. The carrier gas for DUNE is argon, and the trace gases of interest are oxygen ($O_2$), water ($H_2O$), and nitrogen ($N_2$). $O_2$ and $H_2O$ affect the electron lifetime in LAr and must be kept below 0.1 ppb ($O_2$ equivalent) while $N_2$ affects the efficiency of scintillation light production at levels higher than 1 ppm. The argon is sampled from either the argon vapor in the ullage or from the LAr by using small diameter tubing run from the sampling point to the gas analyzer. Typically, the tubing from the sampling points are connected to a switchyard valve assembly used to route the sample points to the desired gas analyzers (see Figure 8.23).

The gas analyzer would be predominantly used during three periods:

1. Once the detector is installed and after the air atmosphere is eliminated from the cryostat to levels low enough to begin cool-down. This purge and gas recirculation process is detailed in Section 8.4.5.3. Figure 8.24 shows the evolution of the $N_2$, $O_2$, and $H_2O$ levels from gas analyzer data taken during the purge and recirculation stages of the DUNE 35 ton prototype

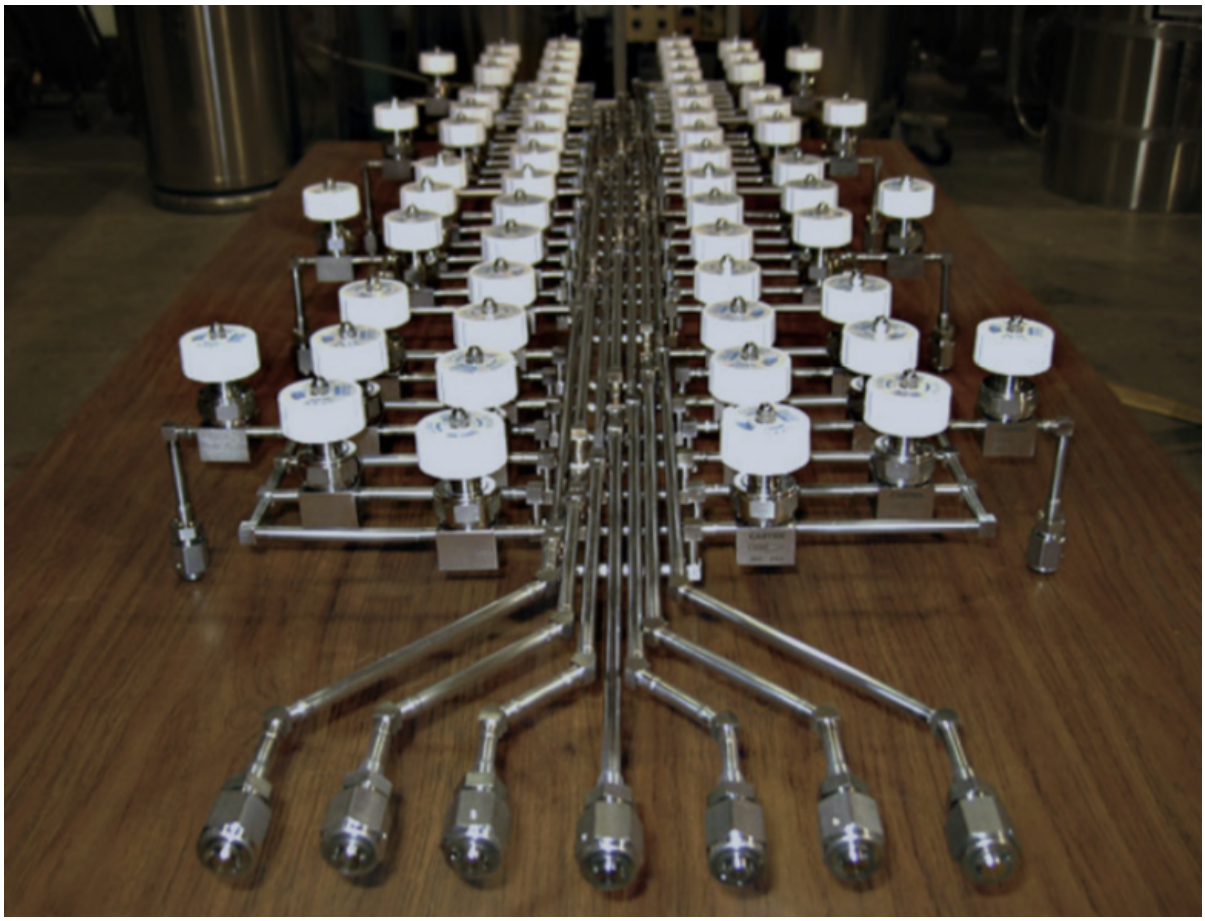

Figure 8.23: A gas analyzer switchyard that routes sample points to the different gas analyzers.

phase 1 run.

2. Before other means of monitoring impurity levels (e.g., purity monitors, or TPC tracks) are sensitive, to track trace $O_2$ and $H_2O$ contaminants from tens of ppb to hundreds of ppt. Figure 8.25 shows an example plot of $O_2$ levels at the beginning of LAr purification from one of the later 35 ton prototype HV runs.

3. During cryostat filling to monitor the tanker LAr delivery purity. This tracks the impurity load on the filtration system and rejects any deliveries that do not meet specifications. Specifications for the delivered LAr are in the 10 ppm range per contaminant.

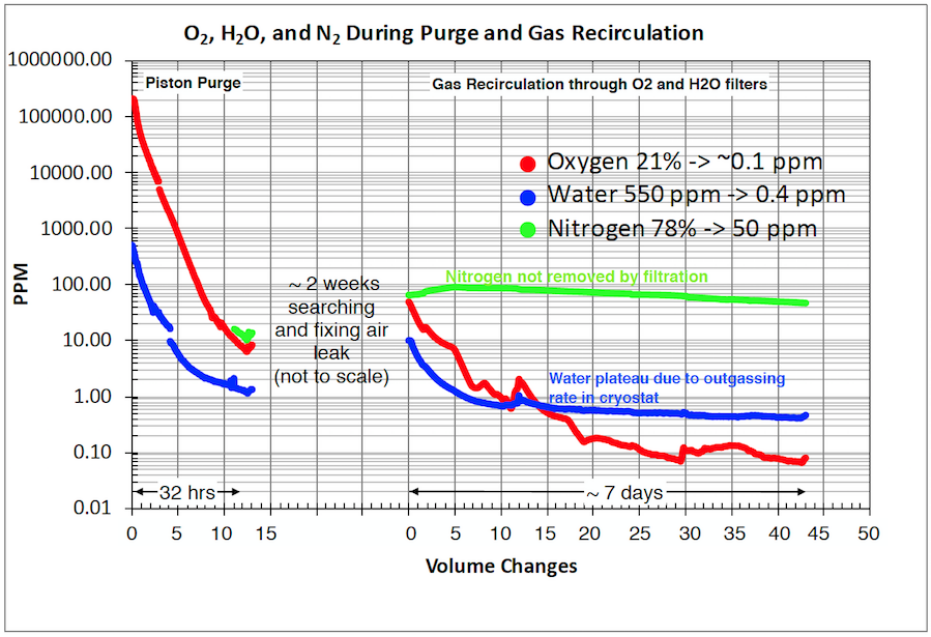


Figure 8.24: Plot of the $O_2$, $H_2O$, and $N_2$ levels during the piston purge and gas recirculation stages of the 35 ton prototype Phase 1 run

Since any one gas analyzer covers only one contaminant species and a range of 3 to 4 orders of magnitude, several units are needed both for the three contaminant gases and to cover the ranges seen between cryostat closure and the beginning of TPC operations: 20 % to $\lesssim$ 100 ppt for $O_2$, 80 % to $\lesssim$ 1 parts per million (ppm) for $N_2$, and $\sim$ 1 % to $\lesssim$ 1 ppb for $H_2O$. Because the total cost of these analyzers exceeds \$100 k, we want to be able to sample more than a single location or cryostat with the same gas analyzers. At the same time, the tubing run lengths from the sample point should be as short as possible to maintain a timely response for the gas analyzer. This puts some constraints on sharing devices because, for example, argon is delivered at the surface, so a separate gas analyzer may be required there.

### 8.2.6 Cameras

Cameras provide direct visual information about the state of the detector module during critical operations and when damage or unusual conditions are suspected. Cameras in the WA105 DP

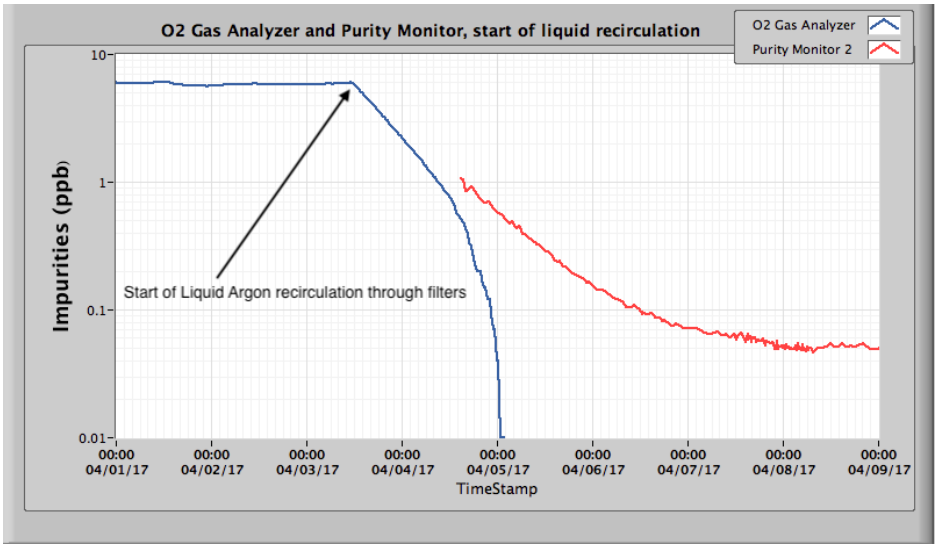


Figure 8.25: $O_2$ as measured by a precision $O_2$ analyzer just after the 35 ton prototype cryostat was filled with LAr, continuing with the LAr pump start and beginning of LAr recirculation through the filtration system. As the gas analyzer loses sensitivity, the purity monitor can pick up the impurity measurement. Note that the purity monitor is sensitive to both $O_2$ and $H_2O$ impurities giving rise to its higher levels of impurity.

demonstrator showed spray from cool-down nozzles and the level and state of the LAr as it covered the charge-readout plane (CRP) [165]. A camera was used in the LAPD cryostat[164] to study HV discharges in LAr and in EXO-100 while a TPC was operating [166]. Warm cameras viewing LAr from a distance have been used to observe HV discharges in LAr in fine detail [167]. Cameras are commonly used during calibration source deployment in many experiments (e.g., the KamLAND ultra-clean system [168]).

In DUNE, cameras will verify the stability, straightness, and alignment of the hanging TPC structures during cool-down and filling; ensure that no bubbling occurs near the GPs (SP) or CRPs (DP); inspect the state of movable parts in the detector module (calibration devices, dynamic thermometers); and closely inspect parts of the TPC after any seismic activity or other unanticipated event. For these functions, a set of fixed cold cameras are used; they are permanently mounted at fixed points in the cryostat for use during filling and commissioning, and a movable, replaceable warm inspection camera can be deployed through any free instrumentation flange at any time during the life of the experiment.

Eleven cameras were deployed in ProtoDUNE-SP at the locations shown in Figure 8.26. They successfully provided views of the detector during filling and throughout its operation.

The following sections describe the design considerations for both cold and warm cameras and the associated lighting system. ProtoDUNE-SP camera system designs and performance are also discussed. The same basic designs can be used for both the SP module and the DP module.

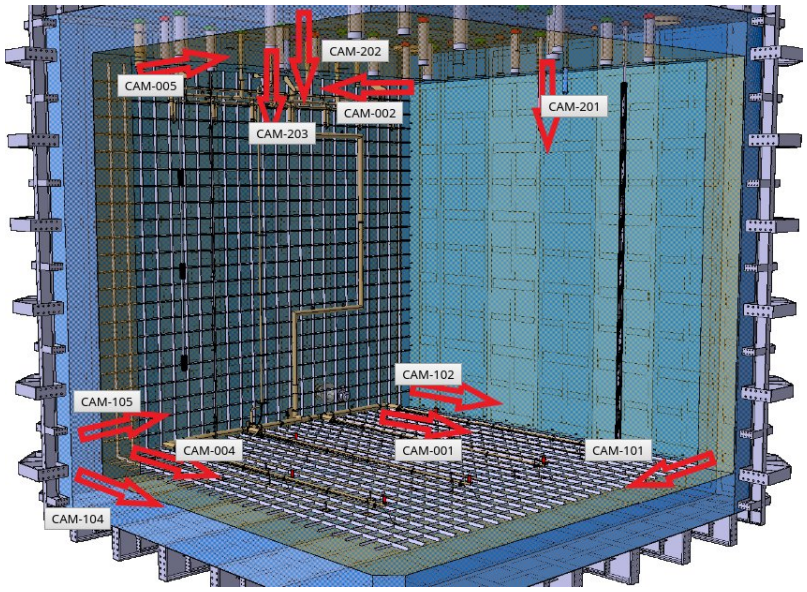


Figure 8.26: A 3D view showing the locations of the 11 cameras in ProtoDUNE-SP.

#### 8.2.6.1 Cryogenic Cameras (Cold)

The fixed cameras monitor the following items during filling:

- positions of corners of APA, cathode plane assembly (CPA), FCs, GPs (1 mm resolution);
- relative straightness and alignment of APA, CPA, and FC ($\lesssim 1$ mm);
- relative positions of profiles and endcaps (0.5 mm resolution); and
- the LAr surface, specifically, the presence of bubbling or debris.

One design for the DUNE fixed cameras uses an enclosure similar to the successful EXO-100 design [166], which was also successfully used in the LAPD and ProtoDUNE-SP (see Figure 8.27). Cameras 101, 102, 104, and 105, shown in Figure 8.26, use this enclosure. A thermocouple in the enclosure allows temperature monitoring, and a heating element provides temperature control. SUB-D connectors are used at the cryostat flanges and the camera enclosure for signal, power, and control connections.

An alternative design uses an acrylic enclosure. This design was used successfully in ProtoDUNE-SP (see Figure 8.27, bottom left). Cameras 001, 002, 004, and 005, shown in Figure 8.26, use acrylic enclosures. All operate successfully, including those at the bottom of the cryostat. The FD modules will be twice as deep as ProtoDUNE, and therefore cameras observing the lowest surfaces of the FC must withstand twice the pressure.

Improved designs for the cold cameras will be tested in ProtoDUNE-DP and CITF for improved imaging including focus adjustment, and in CITF for pressure resistance, during 2020.

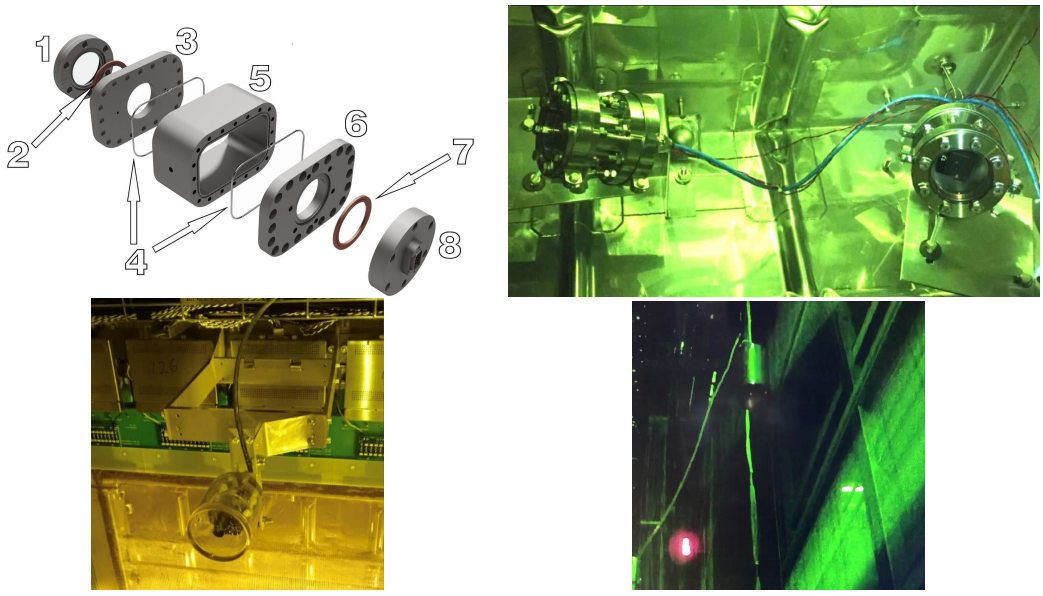


Figure 8.27: Top left: a CAD exploded view of a vacuum-tight camera enclosure suitable for cryogenic applications [166]. (1) quartz window, (2 and 7) copper gasket, (3 and 6) flanges, (4) indium wires, (5) body piece, (8) signal feedthrough. Top right: two of the ProtoDUNE-SP cameras using a stainless steel enclosure. Bottom left: one of the ProtoDUNE-SP cameras using acrylic enclosure. Bottom right: a portion of an image taken with ProtoDUNE-SP camera 105 showing a purity monitor mounted outside the APA on the beam left side. This photo was taken with ProtoDUNE-SP completely filled.

#### 8.2.6.2 Inspection Cameras (Warm)

The inspection cameras are intended to be as versatile as possible. The following inspections have been identified as likely uses:

- status of HV feedthrough and cup,
- status of FC profiles, endcaps (0.5 mm resolution),
- vertical deployment of calibration sources,
- status of thermometers, especially dynamic thermometers,
- HV discharge, corona, or streamers on HV feedthrough, cup, or FC,
- relative straightness and alignment of APA, CPA, and FC (1 mm resolution),
- gaps between CPA frames (1 mm resolution),
- relative position of profiles and endcaps (0.5 mm resolution), and
- sense wires at the top of outer wire planes in SP APA (0.5 mm resolution).

Unlike the fixed cameras, the inspection cameras must operate only as long as any inspection; the cameras can be replaced in case of failure. It is also more practical to keep the cameras continuously warmer than −150 °C during deployment; this allows use of commercial cameras, e.g., cameras of the same model were used successfully to observe discharges in LAr from 120 cm away [167].

The inspection cameras use the same basic enclosure design as for cold cameras, but the cameras

are mounted on a movable fork so that each camera can be inserted and removed from the cryostat, using a design similar to the dynamic temperature probes: see Figure 8.28 (left) and Figure 8.9. To avoid contaminating the LAr with air, the entire system is sealed, and the camera can only be deployed through a feedthrough equipped with a gate valve and a purging system, similar to the one used in the vertical axis calibration system at KamLAND [168]. The entire system is purged with pure argon gas before the gate valve is opened.

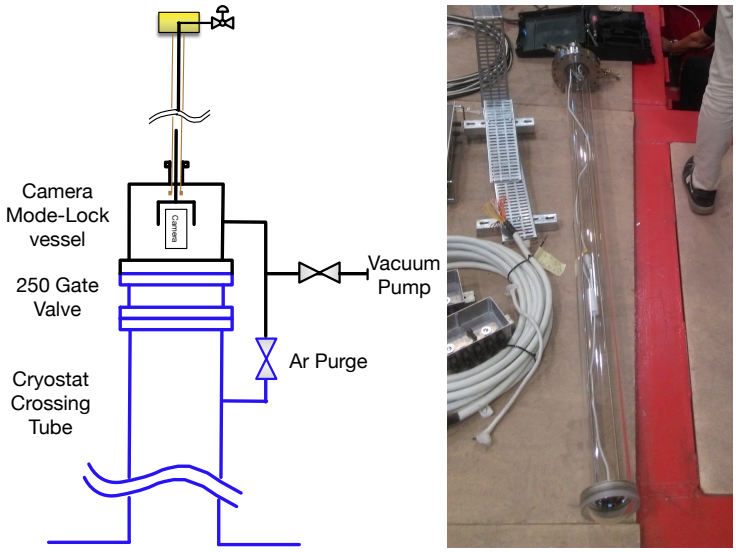


Figure 8.28: Left: An overview of the inspection camera design using a sealed deployment system opening directly into the cryostat. Right: A photo of the ProtoDUNE-SP warm inspection camera acrylic tube, immediately before installation; the acrylic tube is sealed with an acrylic dome at the bottom and can be opened at the top.

Motors above the flange allow the fork to be rotated and moved vertically to position the camera. A chain drive system with a motor mounted on the end of the fork allows the camera assembly to tilt, creating a point-tilt mount that can be moved vertically. With the space above the cryostat flanges and the thickness of the cryostat insulation, cameras can be moved vertically up to 1 m inside the cryostat. The motors for rotation and vertical motion are outside the sealed volume, coupled mechanically using ferrofluidic seals, thus reducing any risk of contamination and allowing manual rotation of the vertical drive if the motor fails.

An alternative design was demonstrated in ProtoDUNE-SP. In this design, the warm camera is contained inside a gas-tight acrylic tube inserted into the feedthrough, so a gate valve or a gas-tight rotatable stage is not needed, and the warm cameras can be removed for servicing or upgrade at any time. Figure 8.28 (right) shows an acrylic tube enclosure and camera immediately before deployment. These acrylic tube enclosures for removable cameras were deployed in ProtoDUNE-SP at the positions marked 201, 202, and 203 in Figure 8.26; they operated successfully. Cameras with fisheye lenses were used in these tubes during initial operation. One camera was removed without any evidence of contamination of the LAr. We plan to use other cameras during post-beam running.

Improved designs for the inspection cameras will be tested in the CITF and ProtoDUNE-SP during 2020 and 2021, focusing particularly on longevity, camera replaceability, and protection of the LAr.

#### 8.2.6.3 Light-emitting system

The light-emitting system uses LEDs to illuminate the parts of the detector module in the camera's field of view with selected wavelengths (IR and visible) that cameras can detect. Performance criteria for the light-emission system include the efficiency with which the cameras can detect the light and the need to avoid adding heat to the cryostat. Very high-efficiency LEDs help reduce heat generation; one 750 nm LED [169] has a specification equivalent to 33 % conversion of electrical input power to light.

While data on how well LEDs perform at cryogenic temperatures is sparse, some studies of NASA projects [170] indicate that LEDs are more efficient at low temperatures and that emitted wavelengths may change, particularly for blue LEDs. In ProtoDUNE-SP, amber LEDs were observed to emit green light at LAr temperature (bottom right photo in Figure 8.27). To avoid degradation of wavelength-shifting materials in the PD system, short wavelength LEDs are not used in the FD; LEDs will be tested in $LN_2$ to ensure their wavelength is long enough.

LEDs are placed in a ring around the outside of each camera, pointing in the same direction as the lens, to illuminate nearby parts of the detector module within the camera's field of view. Commercially available LEDs exist with a range of angular spreads that can be matched to the needs of the cameras without additional optics.

Additionally, chains of LEDs connected in series and driven with a constant-current circuit are used for broad illumination, with each LED paired in parallel with an opposite polarity LED and a resistor (see Figure 8.29). This allows two different wavelengths of illumination using a single chain simply by changing the direction of the drive current, and allows continued use of an LED chain even if individual LEDs fail.

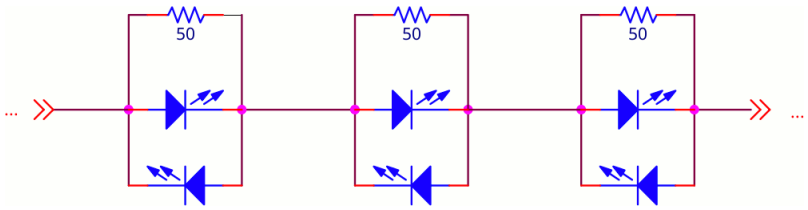


Figure 8.29: Example schematic for LED chain, allowing failure tolerance and two LED illumination spectra.

### 8.2.7 Cryogenics Instrumentation Test Facility

The CISC consortium plans to build a cryogenic instrumentation test facility (CITF) at Fermi National Accelerator Laboratory (Fermilab) to facilitate testing of various cryogenics instrumentation devices and small-scale assemblies of CISC systems. In the past and recent times, various test facilities at Fermilab have provided access to small ($<$ 1 ton) to intermediate ($\sim$ 1 ton) volumes of purified TPC-grade LAr, required for any device intended for drifting electrons for millisecond periods.

The Proton Assembly Building (PAB) facility at Fermilab houses the ICEBERG R&D cryostat and electronics (ICEBERG) 3000 liter cryostat, which enables fast turnaround testing for the DUNE cold electronics (CE).

The PAB facility also includes TallBo (450 liter), Blanche (500 liter), and Luke (250 liter) cryostats. In the recent past, Blanche has been used for HV studies, TallBo for PD studies, and Luke for the material test stand work. These studies have contributed to the design and testing of ProtoDUNE-SP components.

### 8.2.8 Validation in ProtoDUNE

Design validation and testing of many planned CISC systems for the SP module will be done using the data from ProtoDUNE-SP and ProtoDUNE-DP as discussed below.

- Level Meters: The same differential pressure level meters which are already validated in ProtoDUNE-SP will be used in the SP module. The same capacitive level meters currently used in ProtoDUNE-DP will be used in the SP module. These will be validated in the upcoming ProtoDUNE-DP run.
- Pressure Meters (GAr): The same high-precision pressure sensors that are already validated in ProtoDUNE-SP will be used in SP FD.
- Gas Analyzers: The same gas analyzers currently used in ProtoDUNE-SP will be used in the SP module, so they have already been validated.
- High-precision thermometer arrays in LAr: The static and dynamic T-gradient thermometers discussed in the previous sections are validated using ProtoDUNE-SP data.
- Purity Monitors: The same purity monitor basic design used in ProtoDUNE-SP will be used in the SP module. ProtoDUNE-2 at CERN provides opportunities to test any improvements to the design.
- Cameras: various types of cameras are being actively developed in both ProtoDUNE-SP and ProtoDUNE-DP so these detectors will perform validation of the designs. Future improvements can be tested in ProtoDUNE-2 at CERN.

## 8.3 Slow Controls

The slow controls system collects, archives, and displays data from a broad variety of sources and provides real-time status, alarms, and warnings for detector operators. The slow control system also provides control for items such as HV systems, TPC electronics, and PD systems. Data is acquired via network interfaces. Figure 8.30 shows connections between major parts of the slow controls system and other systems.

The ProtoDUNE-SP detector control system[161] fully met its operational requirements. Section 8.3.6 provides a short description of the ProtoDUNE-SP slow controls and its performance.